

Research paper

Cold spray deposition of graded Al-SiC composites



Chunjie Huang^{*}, Alexander List, Levke Wiegler, Matthias Schulze, Frank Gärtner, Thomas Klassen

Institute of Materials Technology, Helmut-Schmidt-University/University of the Federal Armed Forces Hamburg, Hamburg 22043, Germany

ARTICLE INFO

Keywords:

Cold spraying
Graded Al-SiC composites
Powder feed rates
Deposition efficiencies
Mechanical properties

ABSTRACT

Continuously graded materials of Al-based matrix composites reinforced by SiC particles attract increasing attention due to demands for altered thermoelectric and mechanical properties over defined scales. To ensure tailored gradients while avoiding undesirable side reactions, this work focusses on cold spraying as a promising production technique. So far, cold spraying has proved the potential for fabricating aluminum matrix composites with a uniform distribution of reinforcements. The present study explores the direct fabrication of graded composites by applying a constant feed rate of Al powder and gradually increasing feed rates of SiC powder during cold spraying by employing two powder feed lines. The systematic comparison of two SiC powder sizes allows for the identification of common features in composite formation and deducing technical prerequisites for obtaining uniform as well as graded composites. Key issues of microstructural and mechanical investigations concern the attainable hard-phase contents and distributions over the deposit thickness. If a fine hard-phase feedstock powder is used, well-consolidated microstructures with graded SiC distributions are obtained. In case of a coarse hard-phase powder, the layer build-up is less homogeneous. The comparison between the results of the present work and the corresponding literature data reveals similar deposition efficiencies of SiC for co-deposition and the use of pre-mixed powders. However, if cold spraying such blends, the hard-phase contents of the deposits are lower than those of the feedstock powder mix. Furthermore, hard phase contents are lower than for conventional, high-temperature processing techniques. Based on the comparison, the requirements for achieving a wider range of hard phase contents in cold sprayed deposits are elucidated, in particular regarding the feedstock powders and the powder feeder. The acquired understanding can also be transferred to cold spraying of other graded material combinations.

1. Introduction

Silicon-based ceramic materials, such as SiC, can offer low thermal expansion, high wear resistance and high strength at elevated temperatures [1,2], while aluminum alloys have low density, high thermal conductivity, and high toughness [2–4]. Therefore, aluminum matrix composites (AMCs) reinforced with SiC particles (SiC_P) are considered promising materials for functional applications, which can meet favorable combinations of mechanical and thermophysical properties, if the ceramic phase contents within the metallic Al-alloy matrix can be tailored accordingly [2–5]. However, so far, mainly monolithic composites with macroscopically homogeneous phase distributions have been applied that are often inadequate for challenging situations, which require combinations of different properties within one part [2,3]. By systematic and controlled variation of the SiC_P volume fractions, graded

composites with tuned properties can be conceived for a variety of potential applications, covering structural and electronic components [3–5].

For manufacturing of such graded microstructures, various methods were employed that either follow liquid-state routes, such as centrifugal casting [4–7], squeeze infiltration [8], or powder metallurgy-based sintering processes [9,10] and possibly hot pressing [11]. In addition, deposition techniques were employed, including thermal spraying [12], slurry disintegration-deposition [13], and laser melting injection [14]. One common feature of these processes concerns hot processing of a premixed blend of Al and SiC powders. These steps involve the melting of the Al matrix or sintering at temperatures close to the melting temperature. Although a graded distribution of SiC_P was successfully achieved, the state-of-the-art high-temperature processes are associated with the incorporation of defects, such as porosity, oxide inclusions,

* Corresponding author.

E-mail address: huangc@hsu-hh.de (C. Huang).

local phase transformation, and possible complex chemical reactions between the Al matrix and the reinforcements, as well as clustering and degradation of the reinforcement particles [4,10,12,14], which all will significantly influence the material properties and limit its flexibility in applications.

By operating in solid-state and minimizing thermal influences on the spray materials and build-up deposits, cold spraying (CS) of the AMC materials can avoid defects caused by high-temperature treatments thus resulting in solid-bonded interfaces [15–32]. To date, many pioneering attempts have been carried out to use the pre-blended metal/ceramic powders for producing AMCs, such as Al-SiC_P [18–25], Al-Al₂O₃ [25–31], and Al-TiN_P [32]. Based on literature reviews [33–35], the main features of cold sprayed composite materials with respect to classifications of reinforcement materials and their effect on cold sprayed Al matrix composites can be summarized in the following. The mechanical, friction/wear, and thermal properties of deposited materials strongly depend on their microstructures and reinforcement particle contents [18,19,21,22,26–28,30–35]. For example, Sansoucy et al. [19] reported that a wide range from 20 to 60 vol% of SiC volume fractions in the initial blends with Al12Si alloy powder results in fewer amounts covering a small range of 10–20 vol% SiC in the deposits. Nevertheless, in reference to pure Al12Si, the microhardness of cold sprayed deposits was improved from 145 to 205 HV_{0.3}. By using similarly blended feedstock powders, Yandouzi et al. [20] demonstrated that using a pulsed gas-dynamic spraying process could improve the SiC_P fractions of Al12Si-SiC composites up to 14–41 vol%. Similarly, Yu et al. [21] achieved high SiC_P contents ranging from 21.2 to 41.4 vol% in cold sprayed Al5056-SiC_P deposits by using SiC_P contents in the pre-mixed powders of 15–60 vol%. This reduced the wear rate by more than a factor of five in comparison with pure metallic deposit. In addition, the cohesive strength of these deposits was determined to be 107, 147, and 113 MPa, respectively corresponding to SiC_P contents of 0, 26.4, and 41.4 vol%. Eesley et al. [18] found that SiC_P contents in pure Al matrix in the range of 30–40 vol% can substantially reduce the thermal expansion of the deposit. According to the above examples, the mechanical, tribological, and thermal properties can be correlated with the contents of reinforcement particles being present in the composite deposits. In these studies, it is also demonstrated that the deposition efficiencies (DEs) of SiC_P reinforcement depend on the process parameters and the type of Al matrix, as well as on the percentage of ceramic particles in the initial mixture.

In the above cases, CS of monolithic AMCs often necessitates a homogeneous pre-mixing of powders prior to spraying. Using two independent powder feeders during cold spraying offers two advantages. On the one hand, powder premixing as an additional process step could be avoided. On the other hand, the composition can be varied by feed rates for individual deposit layers to obtain graded microstructures and properties. In this study, two different particle size distributions of SiC powders were used. The feed rates of SiC_P were varied for achieving different amounts of SiC_P fractions within the Al-alloy matrix. The contents and distribution of SiC_P within homogeneous and graded composites were determined by microstructural investigations and correlated with measured mechanical properties by powder sizes and individual feed rates. This allows deriving effective guidelines for the fabrication of graded Al-SiC_P composites by cold spraying.

2. Materials and experimental methods

2.1. Materials

Two SiC_P powders in size definitions F220 and F280 (CharpauS, Germany) were individually co-deposited with pure Al powder (TLS Technik GmbH & Co., Germany) on 4 mm thick Al-alloy plates (size of 50 mm × 70 mm) for the composite fabrication. The substrate surface was used in its as-received state and just cleaned with ethanol before cold spraying. The particle size distribution was measured by laser

scattering using an instrument type LA-910 (Horiba, Japan). Details on the particle sizes are given in Fig. 1. The coarse SiC-F220 and fine SiC-F280 powders show a rather broad size distribution with mean particle sizes (D50) of 74 µm and 45 µm, respectively, and are designated as SiC_{CP} and SiC_{FP}. The Al powder has a mean size (D50) of 40 µm and a comparably narrow size distribution.

2.2. Cold spraying

A micron-sized brittle ceramic particle does not plastically deform during cold spraying deposition, and only shows rebound or fragmentation upon impact [36]. Al particles can act as a binder allowing reinforcement particles to be incorporated. Thus, cold spraying parameter selection has to be tuned for Al. Based on empirical data, the process gas temperature was restricted to 500 °C to avoid the risk of nozzle clogging. Respective fine-tuning of the parameter sets was analyzed by using the KSS software (Kinetic Spray Solution, Germany) and set to a process gas temperature of $T_{gas} = 500$ °C and a process gas pressure of $p_{gas} = 3$ MPa. Based on numerical calculations, the ratio between particle impact velocity (v_{imp}) and critical velocity (v_{crit}) at a certain particle impact temperature can be defined as a deposit quality parameter [15,16].

$$\eta = v_{imp} / v_{crit} \quad (1)$$

As calculated by KSS software, a pure Al deposit can be processed at $\eta = 1.38$ at the selected spray parameter sets. More details on the calculations are given as Supplementary material, Section 1.

Cold spraying was performed with a commercially available Impact 5/11 spraying system (Impact Innovations, Germany). A SiC nozzle of type 'out 1' (Impact Innovations, Germany) with a converging-diverging (de-Laval) shape was utilized for the deposition experiments. Its expansion ratio and length are 5.6 and 160.0 mm, respectively. A sketch of the layout and geometric dimensions is shown in Supplementary Fig. S1. Nitrogen was used as the carrier and process gas. The total powder injection distance from powder inlet to nozzle throat was set to 68.9 mm to avoid the nozzle clogging by excessive powder preheating. The spraying distance, the line traverse speed, and the distance between spray lines were kept fixed at 30 mm, 250 mm/s and 2 mm, respectively. Individual details on the spraying parameters used for the fabrication of all samples are summarized in Table 1.

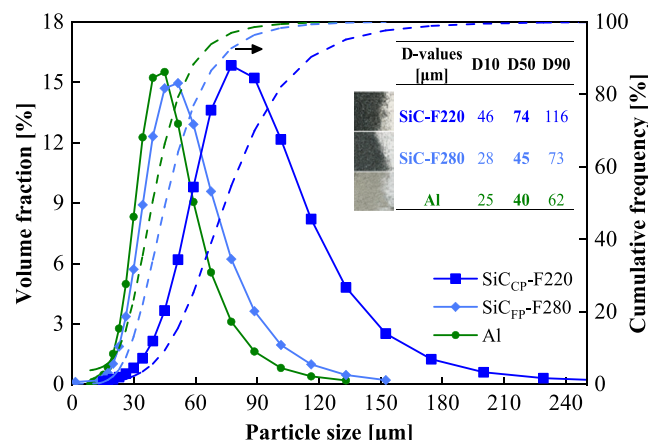


Fig. 1. Size distributions of the SiC_P and the Al-powders as measured by laser diffractometry (the inserted images show the macroscopic appearance of the powders, revealing the dark and white colors for SiC and Al powders, respectively). Key data on size distributions (D10, D50 and D90) are given in the inserted table, referring to sizes for 10 %, 50 % or 90 % volume content of the whole size distribution.

Table 1

Cold spraying parameter sets used in the present set of experiments.

Parameter	Values
Standoff distance, mm	30
Pre-chamber length, mm	-35
Process/carrier gas	nitrogen
p_{gas} , MPa	3
$T_{\text{gas}}, ^\circ\text{C}$	500
Nozzle traverse speed, mm/s	250
Line distance, mm	2

2.3. Compositional designs for aluminum matrix composites

Fig. 2a illustrates a schematic of the cold spraying process to deposit Al matrix composites by using two powder feed lines. By applying a constant delivery rate (5 rpm) of Al powder feeder and a range of delivery rates (i.e., from 0 to 3 rpm) of SiC_P powder feeder, different microstructural configurations within the deposits can be achieved, as sketched in Fig. 2b for four-layer deposition of pure Al in b₀, homogeneous composites (Al-SiC_P) in b₁, b₂ and b₃, as well as graded composites (GM_S/Al-SiC_P) in b₀₋₃.

For comparing individually adjusted feed rates for Al and SiC_P with final compositions in the deposits and estimating individual deposition efficiencies, the delivery rates of the two powder feeders were converted into powder feed rates by using powder tap densities of the feedstock for calibration. With that, individual powder mass feed rates are given as a function of the real powder volume, i.e.,

$$dm/dt = dV \times \frac{\rho}{dt} \quad (2)$$

where m is the powder mass, V is the powder volume, ρ is powder physical density. The powder volume, and its packing density (φ), can be formulated as,

$$dV/dt = \varphi \times V_f \times \frac{dn}{dt} \quad (3)$$

$$\varphi = \rho_t / \rho \quad (4)$$

where the V_f is the volume of the feed disk, n is the revolution speed of the disk, and ρ_t is the powder tap density. Details on these estimates are given in Supplementary material, Section 3–6.

In comparison with SiC_P contents in deposits according to micrographs, the SiC_P volume fractions (A) within the nozzle can be normalized to the feed rates as a function of ρ (powder physical density).

Table 2

Adjusted powder feed rates and nominal SiC_P volume fractions of SiC_P according to the powder delivery rates by using the set-up conditions of the present work.

Powder designation	Delivery rate [rpm]		Mass feed rate [g/min]		Nominal SiC _P fraction [vol%]	Layers
	Al	SiC _P	Al	SiC _P		
Al	5	0	23.9	0	0	4
Al-SiC _{CP1}	5	1	23.9	4.7	14.2	4
Al-SiC _{CP2}		2		9.4	24.9	
Al-SiC _{CP3}		3		14.2	33.3	
GM/Al-SiC _{CP}	0–3		0–14.2		–	
	*					
Al-SiC _{FP1}	5	1	23.9	4.6	13.9	4
Al-SiC _{FP2}		2		9.2	24.5	
Al-SiC _{FP3}		3		13.8	32.7	
GM/Al-SiC _{FP}	0–3		0–13.8		–	
	*					

* SiC_P powder feeder delivery rates for GM/Al-SiC_P: Layer 1 (0), Layer 2 (1 rpm), Layer 3 (2 rpm) and Layer 4 (3 rpm)

Table 2 summarizes the estimated powder feed rates and the corresponding nominal volume fractions (A_n) of SiC_P contents.

2.4. Microstructural characterizations

For a panoramic overview, the distinctive patterns on the deposit surface of as-sprayed samples were visualized by a digital optical microscope (OM) of type VHX-6000 (Keyence, Japan). Cross-sectional microstructures of the samples showing the integration of SiC_P into the Al matrix were analyzed by OM using a DM400M (Leica, Germany). The approximated data of the measured contents and the sizes (equivalent diameter) distribution of SiC_P and the porosities, as well as mean interparticle spacings in the deposits, were determined based on OM cross-section micrographs by using the AxioVision analysis software (dhs Dietermann & Heuser Solution, Germany) and ImageJ 1.52a (NIH, USA), as described in Supplementary material, Section 5. The average particle spacing between SiC_P was assessed according to a 2D nearest neighbor distance (NND) analysis. Particle objects with sizes of less than 20 μm were excluded to avoid local fragmentation effects on the NND and size analyses. The fragmentation of brittle ceramic particles is however not critical in the present work and thus not further assessed. Detailed investigations were further performed by using standard scanning electron microscopy (SEM) with an instrument type Quanta 650 (FEI, Czech Republic), here equipped with a Quantax-200 energy-dispersive X-ray (EDS) micro-analysis system (Bruker Billerica, USA). The backscattering electron (BSE) mode of SEM was used to reveal

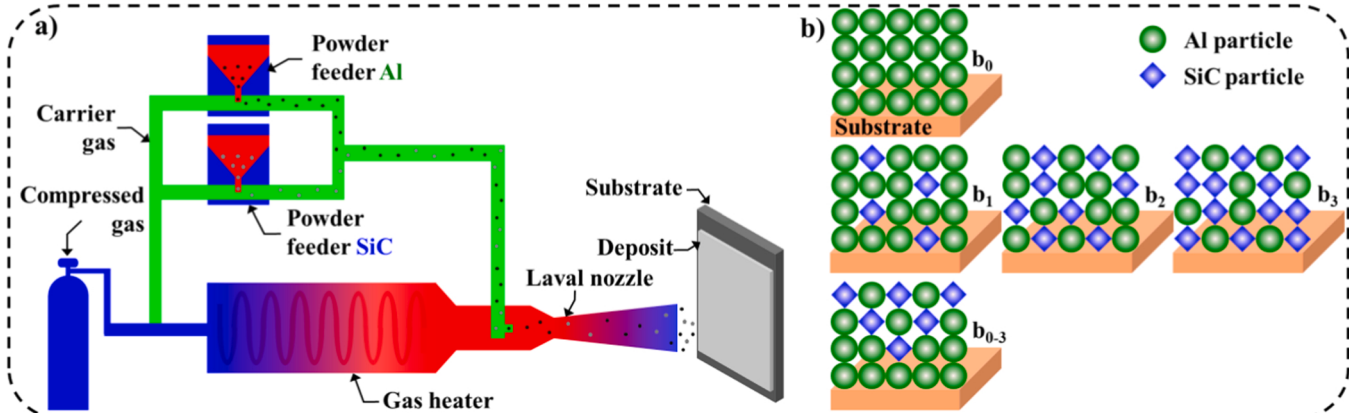


Fig. 2. Schematic illustrations of the CS deposition of composites by using two powder feed lines: (a) main components of spraying system equipped with two powder feeders (more technical details of real powder feeders are given in Supplementary Fig. S2a), and (b) schematics for three types of deposits, i.e., pure Al in b₀, homogeneous composites (Al-SiC_P) in b₁, b₂ and b₃ and graded composites (GM_S/Al-SiC_P) in b₀₋₃. The subscript characters in (b) represent the corresponding delivery rates of the SiC_P powder feeder.

microstructural details as hard phase distribution.

2.5. Analyses of functional properties

Electrical conductivities and related thermal conductivities are functional properties that can be tuned for electronic applications. In addition, electrical conductivity has proven an easy tool for investigating deposit quality in cold spraying [15]. In the present case, the electrical conductivities were measured on the polished surface using an inductive device of type Sigmascop SMP 10-HF a sensor type ES40HF (Helmut Fischer, Germany). The results were averaged from twenty different deposit surface areas to ensure statistical reliability. With volume fractions A_{SiC} and A_{pore} and specific electrical conductivity σ_{El} of pure Al deposit, respectively, the electrical conductivity of the composites can be assumed by parallel circuits, summing up over the individual conductivities, weighted according to the volume fractions:

$$\sigma_{El,comp,parallel} = A_{Al} \cdot \sigma_{El,Al} + A_{SiC} \cdot \sigma_{El,SiC} + A_{pore} \cdot \sigma_{El,pore} \quad (5)$$

In the present case, SiC_p or pore are assumed as isolators in a parallel connection. The real data with this model approach also can provide information about composite microstructures.

Microhardness was determined on the polished cross-sections as HV_{0.3} under a load of 2.942 N according to ASTM E384-10 standard. For each deposit sample, ten indentations were recorded for randomly selected areas using a Vickers hardness testing machine of type ZHU0.2 (Zwick/Roell, Germany). The load of 2.942 N should guarantee that indent size at an expected hardness of about 50 HV_{0.3} results in diagonal widths of ~100 µm and thus average over the composite property.

The mechanical properties of the deposits were investigated by tensile testing in miniaturized dimensions using micro-flat tensile (MFT) specimens of gauge dimensions with a length of 9 mm and a width of 2 mm [15]. For each condition, three specimens in the needed surface finish were prepared by electro spark erosion and later tested. The

specimens were extracted parallel to the spraying line. The stress-strain behavior, and thus material data as the ultimate tensile strength (UTS) were determined by a testing device type Z100 (Zwick/Roell, Germany) by using a constant loading speed according to the standard ISO 6892-1,

$$v \text{ (mm/s)} = 0.00025 \text{ (s}^{-1}\text{)} L_0 \quad (6)$$

where L_0 refers to the defined gauge length of the specimen. Normalized tensile strengths of the different composite deposits can be corrected for the SiC contents for providing more information on bonding at dissimilar interfaces.

$$\text{Normalized UTS} = UTS / (1 - \text{vol.\%SiC}/100) \quad (7)$$

After the complete fracture, the fracture surfaces were investigated by SEM.

3. Results

3.1. Powder morphologies

As given in Fig. 3, overviews and details of the individual surface morphologies of SiC_p and Al feedstock powders were observed by SEM. Fig. 3a-3d depict the typical angular shapes of the crushed SiC powders. According to the literature, such morphology should lead to a higher deposition efficiency as compared to ceramics of spherical shape [31]. Comparing the SEM images at lower magnification (Fig. 3a, 3c), the particle size of the coarse (SiC_{CP}) powder appears to be more homogeneous than that of the fine one (SiC_{FP}). According to random sampling and investigations at higher magnification (Fig. 3b, 3d), no trans-particle cracks were observed in both sizes of SiC particles. Fig. 3e illustrates a uniform size distribution and a spherical shape of the Al feedstock powder. Larger magnifications (Fig. 3f) could reveal some satellites at very few larger particles. Under these conditions of powder

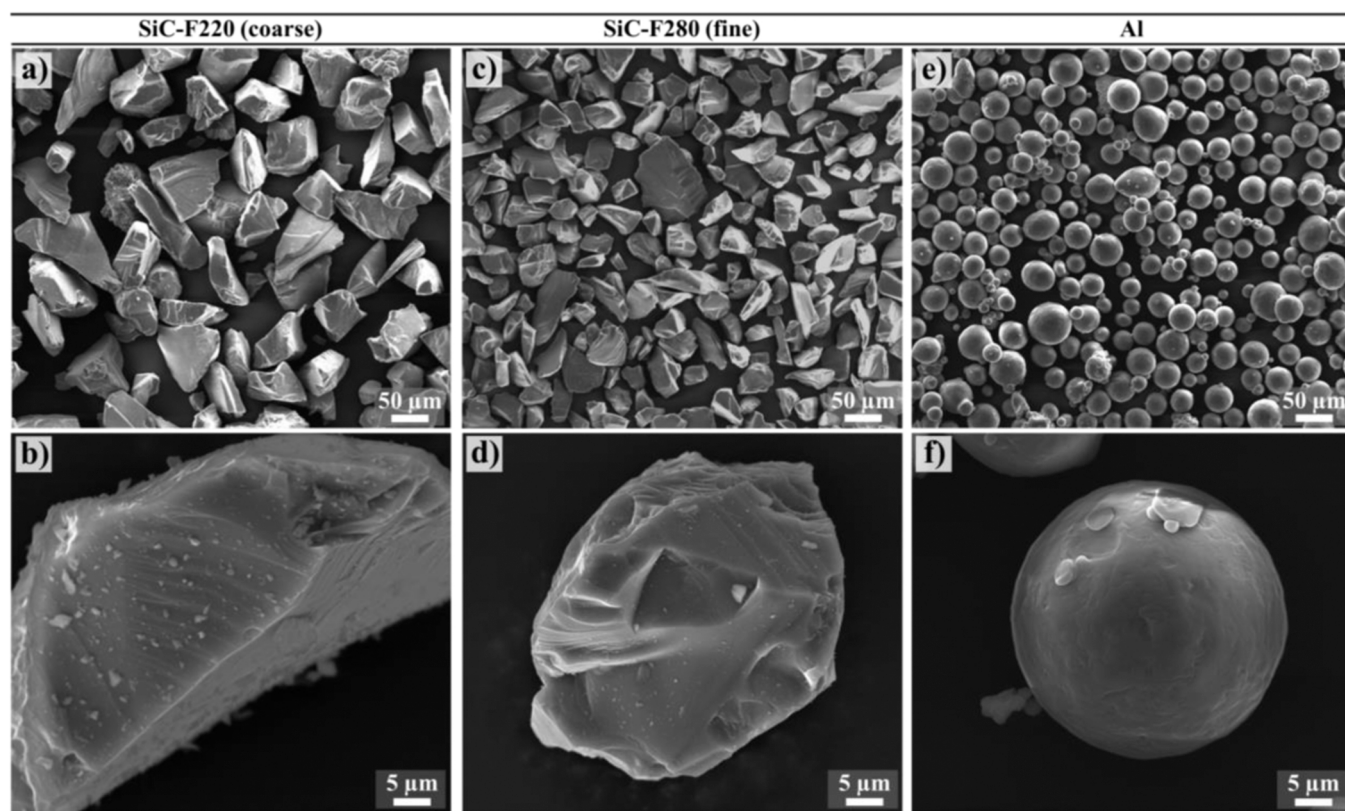


Fig. 3. SEM micrographs showing the morphologies of the coarse SiC-F220 (a and b), fine SiC-F280 (c and d), and Al (e and f) feedstock powders that are used in the cold spraying experiments as overviews (up $\times 500$) and details (down $\times 5000$).

atomization and particle classification, these few defects will not have a significant impact on particle deposition during cold spraying.

3.2. Microstructure of pure Al deposit

As a reference for the influences by co-deposition of composites, pure Al-coating was processed by employing one feed line at a constant delivery rate of 5 rpm. Fig. 4 shows the obtained microstructures by building up to four spray layers according to OM and SEM analyses of the cross-section. The overview in Fig. 4a illustrates rather high coating integrity with a very low porosity of only less than 0.11 %. Due to the high impact velocity (577 m/s for D50 as given in Supplementary section 1), the Al particles undergo intensive plastic deformation upon impact. For the present case of similar materials for substrate and deposition, both should show similar degrees of deformation. The resulting common areas of shear instability under particle impact conditions will determine the bonding characteristics and hence the adhesion strength [15]. As shown by the higher magnification in Fig. 4b, the substrate surface is well deformed allowing for sufficient shape adoption of the highly flattened spray splats. Thus, no interface defects, like cracks, are observed at the deposit-substrate interface. As indicated by Fig. 4c, the general appearance of the deposit does not vary with layer build-up also showing the same degrees of particle deformation and flattening close to the surface. A higher magnification of the coating interior shown in Fig. 4d demonstrates that most of the internal interfaces are well bonded. The details also reveal heterogeneous splat microstructures with higher degrees of deformation close to the vicinity of the internal interfaces (red arrow) and less deformed grains (yellow arrow) within the deposited particles. Even with SEM resolution, only a few non-bonded interfaces (black arrow) can be seen.

3.3. Homogeneous Al-SiC_P composites

3.3.1. Composite surface topographies

Fig. 5 compares the intrinsic surface textures (i.e., surface region S_{low} /region S_{high} , indicating surface areas that contain low and high amounts of SiC_P) of the homogeneous composites that were co-deposited with two SiC_P powder sizes under varying delivery rates. The overall appearances of samples are illustrated by the respective macrographs. In

addition, higher magnifications show individual details. The comparison reveals that deposit surfaces show a distinguishable pattern and are thus less homogenous than expected by the uniform experimental settings in cold spraying. The visible features can be described by the following trends: i) Hard-phase powder sizes have a minor influence on global homogeneity. Using coarse and fine SiC_P powders, similar patterns are obtained at the same delivery rates. The bright areas (indicated by S_{low}) seem to show unexpectedly high Al-contents with only very few incorporated SiC particles. ii) At a low SiC_P delivery rate of 1 rpm (Fig. 5a, 5d) and 2 rpm (Fig. 5b, 5e), roughly and equidistant stripes can be distinguished. Such a frequent surface pattern could be due to step-wise feeding by the distance of feeder holes. A time dt (powder) can be correlated to the dt (coating) needed to travel over one wavelength from hill to hill under the respective robot traverse speed. iii) At increased SiC_P delivery rates, the differences diminish, finally resulting in rather homogenous features, the homogeneity being more prominent for the SiC_{FP} powder. The comparison indicates that, within this parameter regime, the similar sizes and delivery rates between SiC_P and Al powders can allow for a more uniform spatial dispersion.

To gain more information on the co-deposition mechanisms for similar powder sizes of SiC_P (fine) and Al, the surface morphologies (Fig. 6a, 6c) and elemental distributions (Fig. 6b, 6d-6f) of the respective bright and dark patterns (corresponding to S_{low} and S_{high} in Fig. 5d and 5f) were analyzed by SEM using SE and EDS-mapping modes. The following conclusions can be drawn: i) Deposited Al particles in the surface region of S_{low} (Fig. 6a) are less deformed by SiC_{FP} impacts than those in the region of S_{high} (Fig. 6c), corresponding to less coverage by the embedded SiC particles. The Si distributions shown in Fig. 6b and 6d are in good agreement with the observations in Fig. 5d. ii) Small SiC_{FP} particles have a high impact velocity, resulting in severe plastic deformation of the metallic surface and allowing for local embedding into a single soft Al particle (blue arrows in Fig. 6a), while large SiC_{FP} particles have more global influence and cause tamping of the Al matrix (blue arrows in Fig. 6c). iii) At a SiC_{FP} delivery rate of 3 rpm, region S_{low} (Fig. 6e) and region S_{high} (Fig. 6f) show no apparent differences in Si contents, demonstrating the increasing homogeneity in deposits at higher SiC contents.

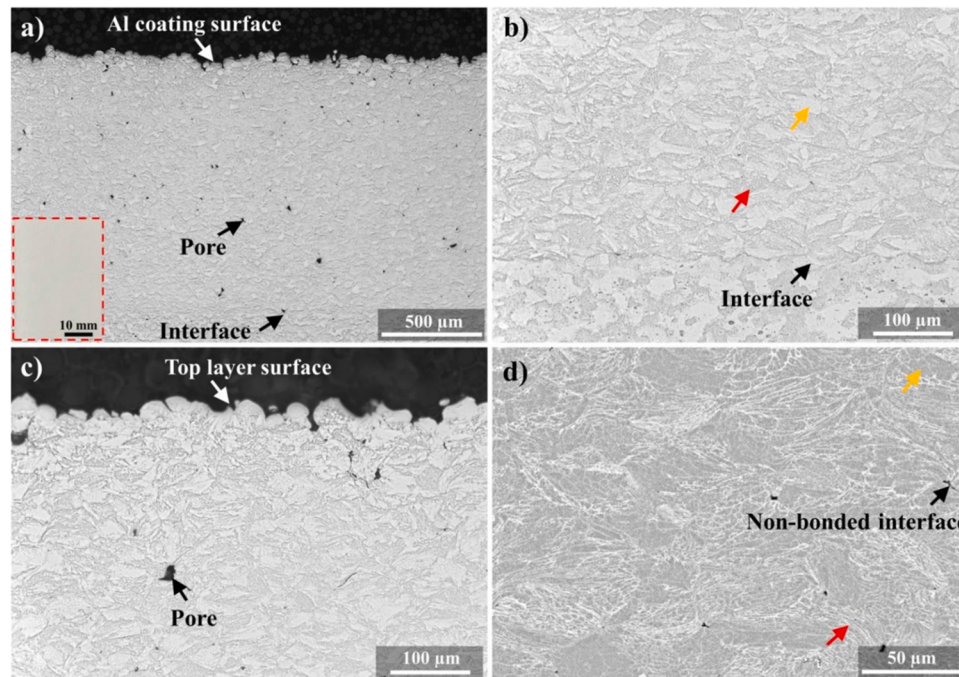


Fig. 4. Micrographs of the reference of the pure Al sample deposited at a constant delivery rate of 5 rpm. (a) overview of the OM microstructure over the entire four-layer deposit, the insert in (a) corresponds to the photographic image of Al deposit surface. (b and c) OM microstructural details at the interface to the substrate and the deposit surface, and (d) high magnification of SEM microstructural detail of the deposit interior. The red and yellow arrows indicate highly and less deformed areas, respectively.

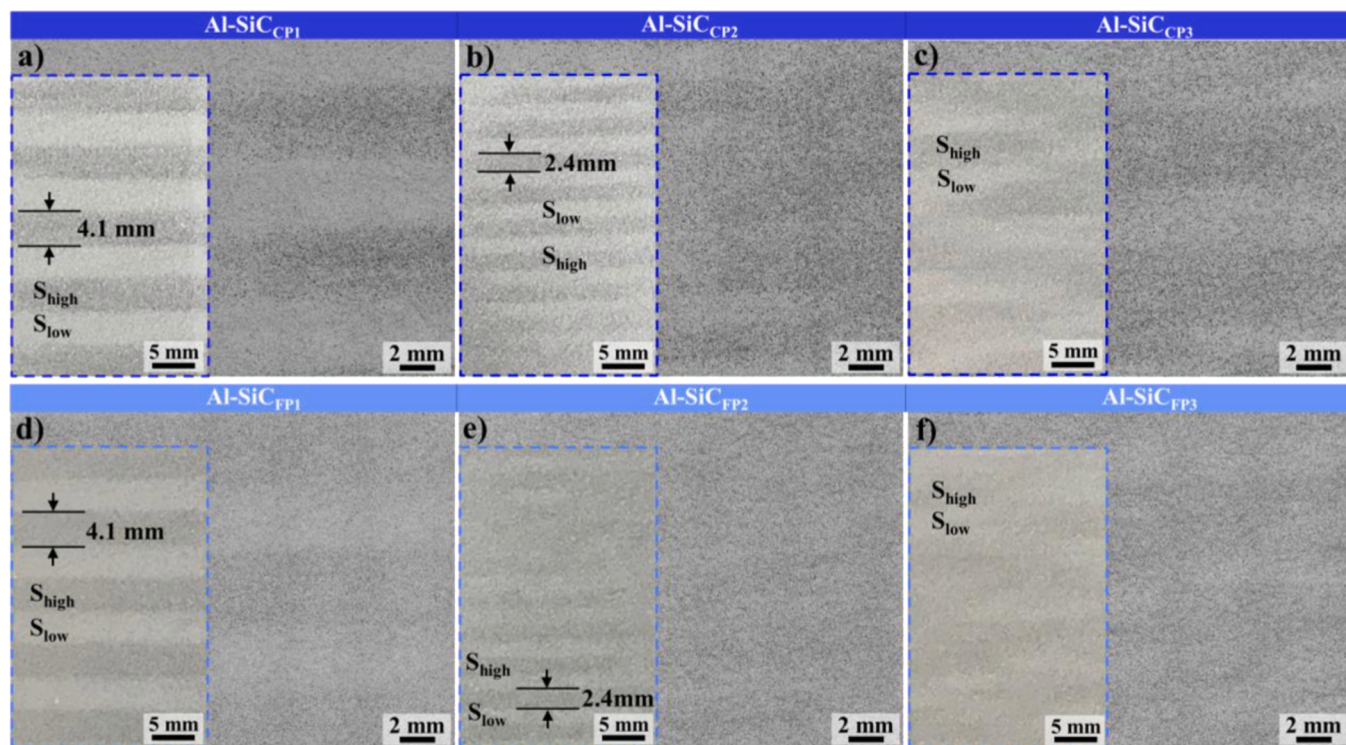


Fig. 5. OM micrographs showing the surface morphologies of the four-layered composites as processed with coarse SiC_{CP} (up) and fine SiC_{FP} (down) hard phase powders by using different delivery rates of SiC_P: (a and d) 1 rpm, (b and e) 2 rpm and (c and f) 3 rpm. The surfaces are shown in two different magnifications for better distinguishing individual patterns. In Fig. 5a-5d, S_{low} and S_{high} indicate the areas that contain low and high amounts of SiC_P.

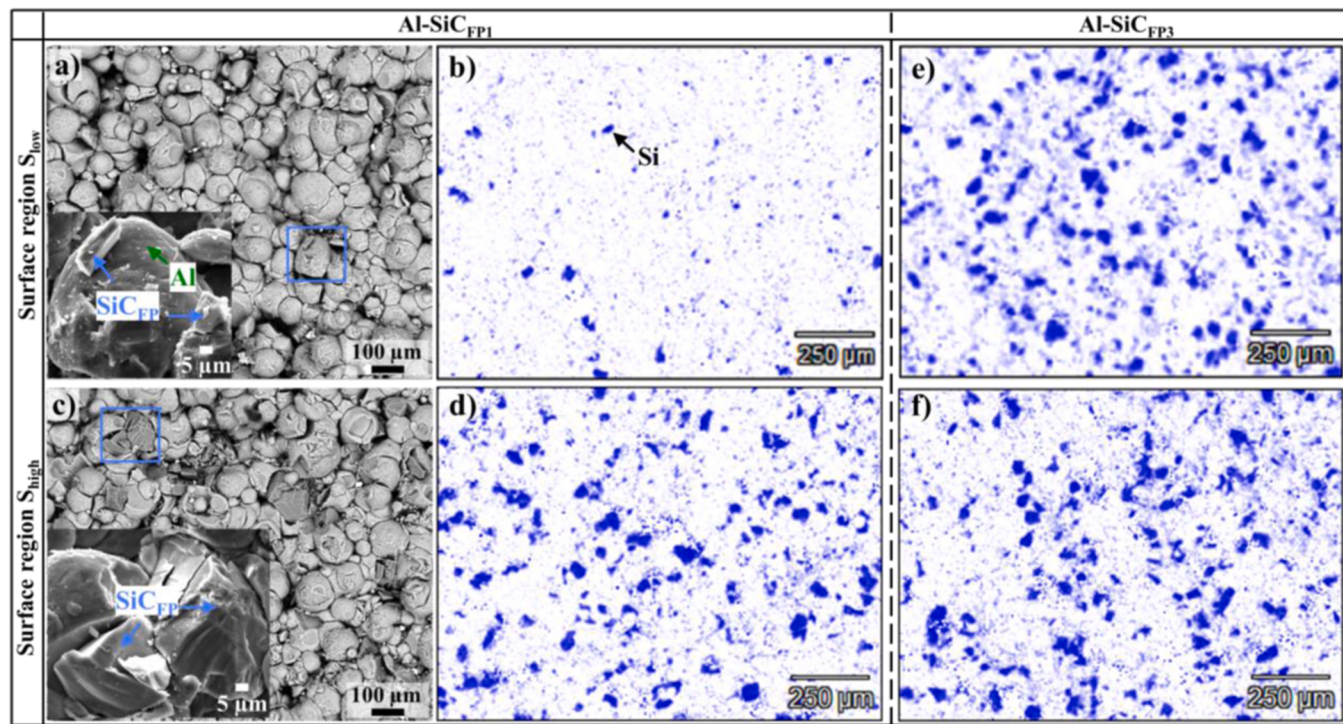


Fig. 6. Surface topographies of Al-SiC_{FP} composites as revealed by SEM in SE and EDS-mapping modes for delivery rates of SiC_P of (a-d) 1 rpm and (e-f) 3 rpm. (a-b) and (c-d) corresponding to the surface region S_{low} and region S_{high} in Fig. 5d, respectively. The insets in (a and c) show SiC_P impacts at higher magnification (corresponding to the blue rectangles). (e and f) correspond to the surface region S_{low} and region S_{high} in Fig. 5f, respectively. EDS mapping was performed by using Si (K α) radiation, locally high SiC contents here being displayed in blue (for interpretation of the references to color in this figure, the reader is referred to the Web version of this article).

3.3.2. Composite microstructures

To investigate the influence of SiC_P powder sizes and delivery rates over two powder feed lines (see Table 2) on composite microstructures, cross-sections of the different four-layer deposits were analyzed by OM and SEM. The microstructural analyses reveal information on deposit homogeneity over deposit thickness, as well as global and local SiC_P distributions and contents within the composite deposits. In the following, examples of deposit microstructures for building-up composites with coarse and fine SiC_P powders are presented in Fig. 7 and 8. Quantitative results are then summarized in Fig. 9.

Fig. 7 shows the cross-sectional microstructure features of $\text{Al}-\text{SiC}_\text{CP}$ samples fabricated at different SiC_CP delivery rates, (a-b) 1 rpm, (c-d) 2 rpm, and (e-f) 3 rpm. The comparison illustrates that the overall $\text{Al}-\text{SiC}_\text{CP}$ content increase with nominal SiC_CP feed rates (refer to Table 2). At the highest SiC_CP feed rate of 14.2 g/min (i.e. 3 rpm), a hard phase content of approx. 21.5 vol% is obtained (see Fig. 9a). However, the SiC_CP distributions are rather non-uniform, particularly for the lower feed rates of 4.7 and 9.4 g/min (1 and 2 rpm).

According to the reports in the literature, a uniform distribution of reinforcement phases in the Al matrix composites improves deposit

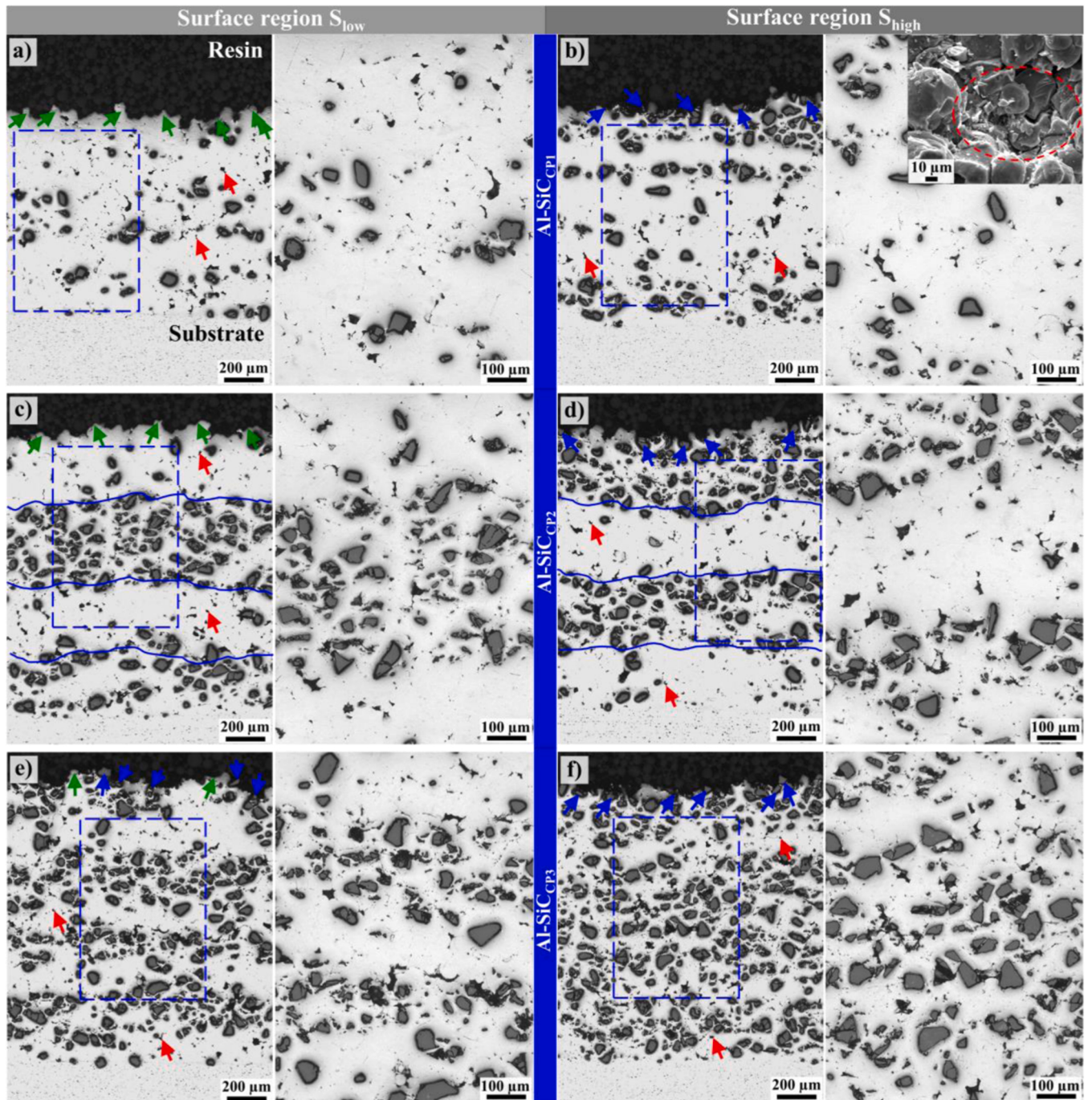


Fig. 7. Microstructural overviews and details (OM micrographs of the cross-sections) of uniformly processed $\text{Al}-\text{SiC}_\text{CP}$ deposits sprayed with different SiC_CP delivery rates. (a-b) 1 rpm, (c-d) 2 rpm and (e-f) 3 rpm, corresponding to SiC_CP feed rates of 4.7 g/min, 9.4 g/min and 14.2 g/min, respectively. Fig. 7a, 7c and 7e, and Fig. 7b, 7d and 7f correspond to region S_{low} and region S_{high} as denoted in Fig. 5a-5c. The arrows indicate different features with blue: SiC_P on the top layer, green: deposited Al particles, and red: pores within the Al-matrix. Blue dashed lines in Fig. 7c-d indicate distinguishable inter-layers. The inset in Fig. 7b shows the local surface topographies of a crater caused by SiC_P impact.

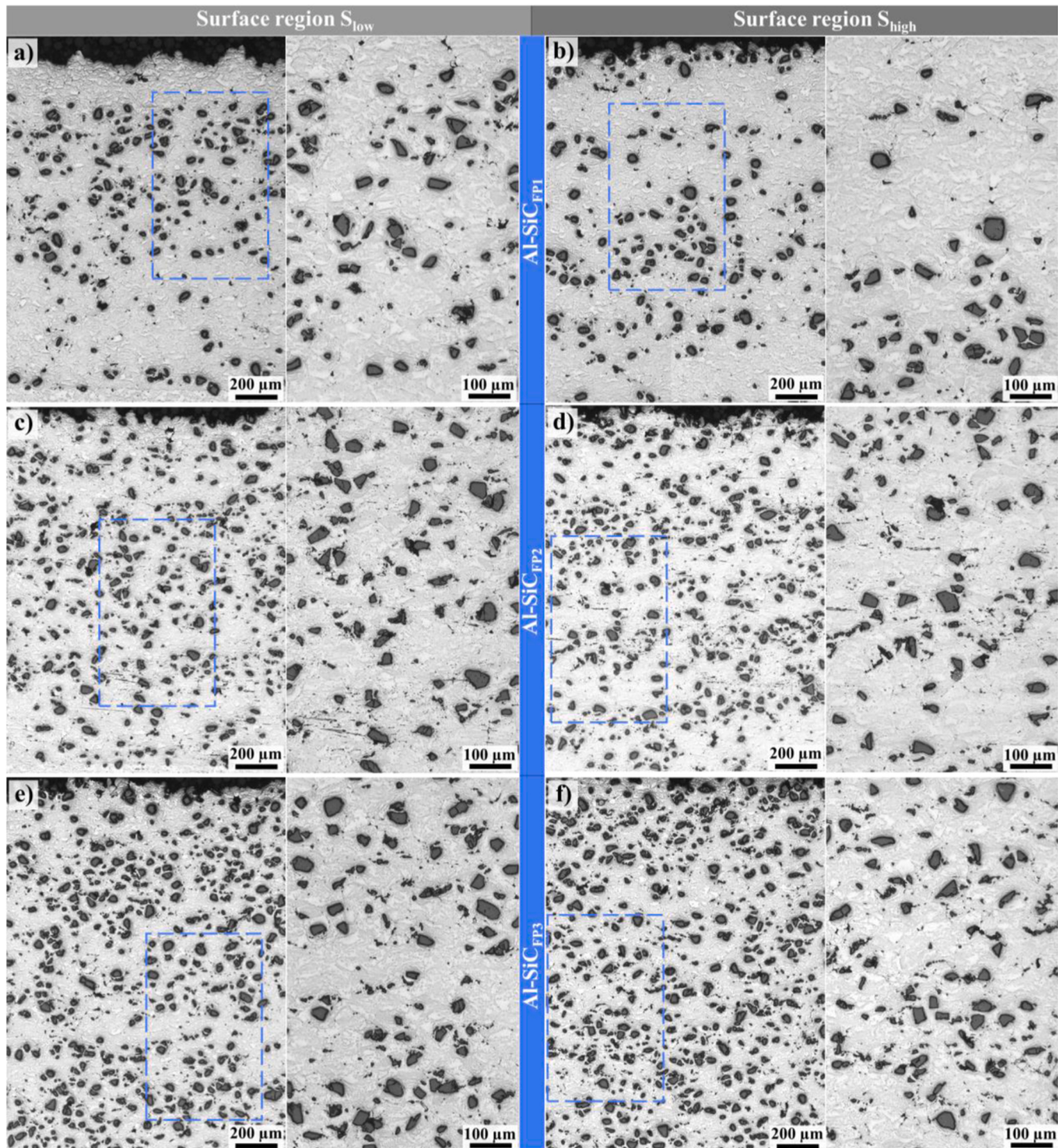


Fig. 8. Microstructural overviews and details (OM micrographs of cross-sections) of uniformly processed Al-SiC_{Fp} samples co-deposited with fixed SiC_{Fp} powder delivery rates of (a-b): 4.6 g/min (1 rpm), (c-d): 9.2 g/min (2 rpm) and (e-f): 13.8 g/min (3 rpm) for surface regions S_{low} (left) and S_{high} (right). The blue rectangles in Figs. a-f indicate areas that are displayed at higher magnification to show details.

microhardness [19–22,25,28,30–32]. Accordingly, local microstructural heterogeneities in Al-SiC_{CP} samples could have a significant influence on deposit performances. For investigating possible influences of feed rate regime, the SiC_{CP} distributions in cross-sections (Fig. 7), corresponding to surface region S_{low} and S_{high} (from Fig. 5) are compared. The following trends can be derived: (i) Regarding the respective surface pattern corresponding to regions S_{low} and S_{high} in Al-SiC_{CP1} and Al-SiC_{CP2} samples, respectively, the top layers show significantly different

populations of deposited SiC_{CP}. i.e., region S_{low} contains a nearly pure Al layer with rather limited amounts of SiC_{CP} (see green arrows in Fig. 7a and 7c). In contrast, surface regions S_{high} show higher SiC_{CP} contents (see blue arrows in Fig. 7b and 7d), which correlates well to the surface observations shown in Fig. 5a and 5b. The insert in Fig. 7b shows the surface topography of the composite based on coarse SiC_p, which can give evidence of a crater by the non-successful SiC_{CP} impacts. (ii) By increasing the SiC_{CP} feed rate from 4.7 to 9.4 g/min, the areas of low and

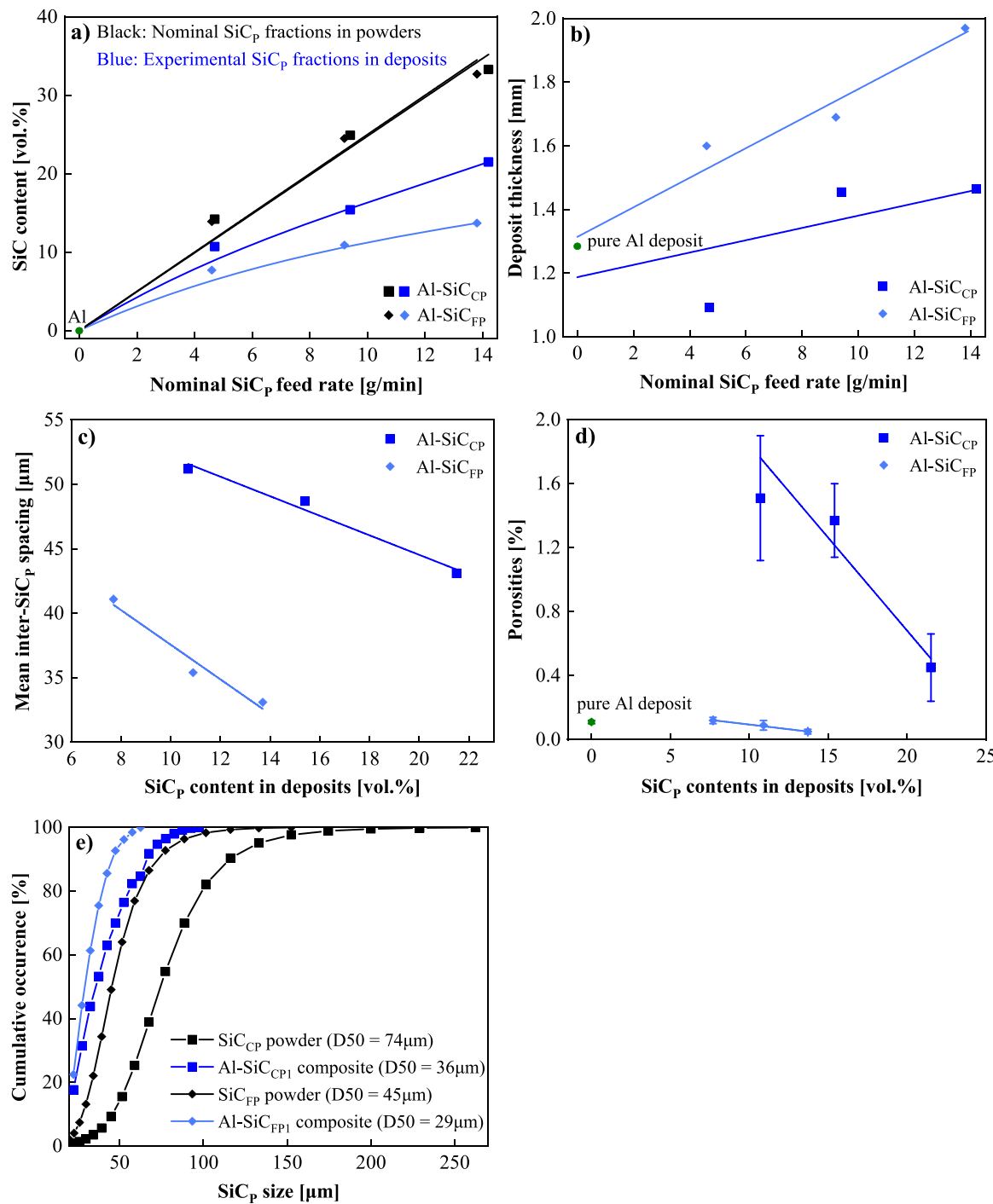


Fig. 9. Correlations between the (a) nominal and measured SiC_P fractions and (b) deposit thickness (corresponding to deposition efficiencies) over the nominal SiC_P feed rates. Correlations between (c) average inter-SiC_P spacing and (d) deposit porosities over the SiC_P contents in deposits. (e) displays the correlation between SiC_P size distributions of Al-SiC_{CP} and Al-SiC_{FP} deposits in comparison to that of the powders.

high SiC_{CP} contents show a rather periodical appearance, as indicated by blue lines in Fig. 7c-d. In contrast to the low amounts of SiC_{CP} in the Al-SiC_{CP1} sample, also more SiC_{CP} appears to be incorporated during the Al-SiC_{CP2} sample deposition, which by overall higher mass could increase deposit thickness (Fig. 9b). (iii) Areas of low and high SiC_{CP} contents are less distinct for the highest feed rate of SiC_{CP3}. As given in Fig. 7e, only very few areas are observed that contain fewer SiC_{CP} in S_{low} region. This confirms that higher SiC_{CP} feed rates promote composite homogeneity.

Fig. 8 presents the microstructures of the Al-SiC_{FP} deposits (left: S_{low}

region, right: S_{high} region) co-deposited with SiC_P feed rates of (a-b): 4.6 g/min (1 rpm), (c-d): 9.2 g/min (2 rpm) and (e-f): 13.8 g/min (3 rpm), according to the areas in Fig. 5d-5f. The microstructures reveal that individual hard-phase contents increase with SiC_P feed rates. At a low SiC_P feed rate of 4.6 g/min (Fig. 8a-8b), the top layer of the deposit shows some inhomogeneity with hard phase depleted areas, similar to the observations from Fig. 7a, 7c. The nearly pure Al layer (Fig. 8a), and the higher SiC_{FP} contents (Fig. 8b), correlate well with the surface observations shown in Fig. 5d. For higher SiC_{FP} feed rates of (9.2 g/min and 13.8 g/min), rather homogeneous deposits are obtained through the

entire thickness of the layers.

As compared to the co-deposition using coarse SiC_P powder (Fig. 7), the maximum local volume content of embedded hard phases is lower than by employing the smaller hard phases (Fig. 9a). However, the incorporation of smaller SiC_P sizes results in lower inter-particle spacing (Fig. 9c). Furthermore, the amount of hard phases also affects the porosity. An increase in SiC feed rate from 4.7 to 14.2 g/min g/min by using coarse SiC powder reduces the composite porosities from about 1.51–0.45 % (Fig. 9d). In contrast, fine SiC powder uniformly leads to dense deposits with rather low porosities, about 0.1 %, and only minor changes with hard phase content. As compared to the deposition of pure Al (Fig. 4b), the spray splats of the Al-matrix within the composites appear more deformed, as demonstrated by lower amounts of less deformed areas in Fig. 8a–8f. In addition, some particle-particle boundaries are decorated with fine SiC_P. As compared to Al-SiC_{CP2} (Fig. 7c–7d), the more uniform distribution of reinforcements through the thickness of Al-SiC_{FP2} appears beneficial for deposit buildup, resulting in a linear increase of deposit thickness with the amount of embedded hard phases (Fig. 8, 9b). By observing the higher magnifications, it is apparent that using rather similar sizes of Al and SiC_{FP2} can enable relatively low porosity composite build-up (~0.09 %), even showing advantages over the Al deposition of Al-SiC_{CP2} deposit (~1.37 %) sprayed at the same parameters (compare Fig. 7, also Fig. 9d). This is attributed to the peening effect of the fine reinforcement particles. Attaining such homogenous phase distribution is a necessary prerequisite for building-up defined graded distributions of SiC_P in specific spray layers. In contrast, by co-deposition using the coarse SiC_P, the desired homogeneity in hard phase distribution is only obtained at higher feed rates.

The results of the global analyses are summarized in Fig. 9. As given in Fig. 9a, the experimentally obtained SiC_P contents are significantly lower than expected by the individually adjusted feed rates. The comparison also shows that deviations are higher for using the fine SiC particle size. The higher SiC contents obtained by higher feed rates result in smaller mean interparticle spacings and porosities (Fig. 9c–9d). Despite the lower hard phase contents as compared to the Al-SiC_{CP} composite, the inter-hard phase spacings are smaller for the Al-SiC_{FP} samples (Fig. 9c). By increasing the volume of material into the system, the deposit thickness increases with SiC_P feed rates, as illustrated in Fig. 9b. However, this trend is not so clear for the coarse SiC_P powder. Interesting information is given by the hard phase sizes (Fig. 9e). As compared to the feedstock with mean sizes D50 of 74 and 45 μm for the coarse (SiC_{CP}) and the fine (SiC_{FP}) powders, the mean hard phase sizes within the Al-SiC_{CP1} and Al-SiC_{FP1} composites declined to 36 and 29 μm, respectively, the ratio between composite and feedstock being

significantly larger for the coarse SiC_P.

3.4. Deposit properties

The following paragraph summarizes results on functional properties such as electrical conductivity, microhardness (both in Fig. 10) and deposit strength (Fig. 11) to provide an estimate of possible use in technical applications. In addition, the different properties provide information on deposit qualities and contributions by similar and dissimilar internal interfaces.

3.4.1. Electrical conductivity

In general, the electrical conductivity of cold sprayed deposits is highly influenced by the microstructural characteristics, such as the amount of porosities and non-bonded particle-particle interfaces, as well as the hard phase contents. The results are shown in Fig. 10a as a function of hard phase contents. In this comparison, the pure Al-deposit shows the highest conductivity, which, however, is lower than that of the respective, fully deformed Al 1050 H18 bulk material (34.5 MS/m). This can be attributed to the presence of non-bonded interfaces. The conductivities of all composite deposits are lower than Al, as expected for incorporating isolators of SiC into the metallic matrix. Within the statistical error, the conductivities of Al-SiC_{FP} samples remain nearly constant with increasing hard phase content. In contrast, the measured conductivities of the Al-SiC_{CP} deposits are lower, indicate a slight decrease with SiC_P contents and show larger scatters. However, for both, the decline with SiC-content is less steep than expected for assuming a parallel connection (Eq. 5) as indicated by the dashed line. The deviation from the model at lower contents of the hard phase might be attributed to defects as non-bonded interfaces in the Al matrix. For higher hard phase contents, the quality of the conductive Al-matrix is then improved, in accordance with the reduced porosities. The differences between the Al-SiC_{FP} and the Al-SiC_{CP} deposits could be due to more defects incorporated into the latter. In addition, the larger scatter of data for Al-SiC_{CP} could be attributed to deposit inhomogeneities caused by locally varying SiC contents and porosities.

3.4.2. Microhardness

Fig. 10b shows the obtained microhardness of pure Al and the Al-SiC composite deposits as a function of SiC contents in deposits. In spite of the different compositions, the hardness varies only slightly between about 48 and 53 HV_{0.3}. For all Al-SiC_{CP} samples, as well as Al-SiC_{FP1} sample with less than about 10 vol% SiC, the hardness of those composites is slightly lower than that of the pure Al-deposit. With higher SiC contents, the composite hardness then is improved for both powder

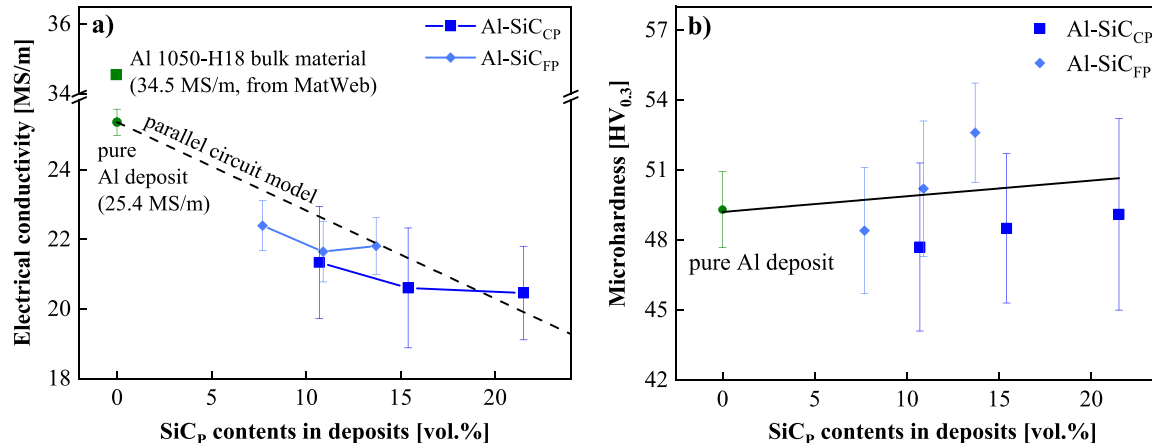


Fig. 10. (a) Measured electrical conductivities of different deposits as a function of the SiC_P. The dashed curve corresponds to the model assuming SiC as isolators in parallel connection (Eq. 5). The conductivity of the Al matrix was set to 25.4 MS/m according to the reference of the deposited pure metal. Data on bulk material is from MatWeb. (b) Microhardness of different deposits as a function of the SiC_P contents.

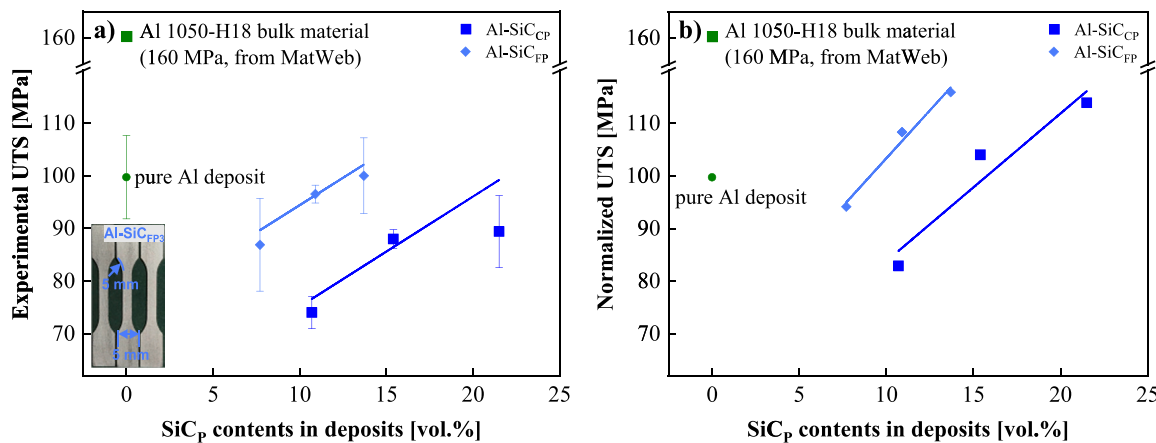


Fig. 11. (a) Experimental and (b) normalized UTS of as-sprayed samples as a function of SiC_p contents in deposits. The insert in (a) shows the macrographic image of the Al-SiC_{FP3} MFT specimens. Dashed lines indicate the variation of nominal tensile strengths (Eq. 7) of the different composite deposits. Data on bulk material is taken from MatWeb.

sizes. However, the hardness increase for Al-SiC_{FP} is steeper than that of Al-SiC_{CP}. Part of that could be attributed to the more homogeneous dispersion of the fine hard phases in the case of Al-SiC_{FP} (Fig. 9c), while higher porosities could account for the lower hardness of Al-SiC_{CP}. In general, different strengthening effects by peening of the Al matrix may be related to a number of hard phase impacts and affected depths. These could also be superimposed by thermal recrystallization of differently working hardened areas during the deposition procedure and layer-by-layer heating by the spray gun. The data can provide a reliable property estimate for varying compositions and thus graded layers.

3.4.3. Tensile strength

The results on UTS are summarized in Fig. 11 as integral composite data in (a) and as normalized data to matrix content in (b). The strength of the pure Al deposit of about 100 MPa is lower than that of a fully working hardening temper condition (160 MPa for Al 1050-H18). The difference could be attributed to the amounts of non-bonded interfaces being present. As compared to the pure Al deposit, the UTS of the cold sprayed Al-SiC is lower. This indicates that most of the carbides do not carry tensile loads, probably due to non well-bonded dissimilar interfaces. However, the strengths of the composites increase with increasing hard phase contents, nearly reaching a range similar to that of the pure Al-deposit. The comparison also shows that at similar hard phase contents, composites on the basis of the fine SiC_{FP} powder reach higher strengths than those containing coarser carbides. The normalized data in Fig. 11b show that the strength of the Al-matrix is reduced at low hard phase contents, probably due to induced non-bonded interfaces. However, the normalized composite strengths (solid fitting lines in 11b)

increase with higher hard phase contents. That might be attributed either to improved bonding within the Al-matrix or load carrying support by the SiC transferred over some amounts of bonded dissimilar interfaces. In this comparison, the overall lower strength of composites containing the coarse SiC_{CP} might be due to the higher amounts of defects (compare porosity) within these composites.

According to the individual stress-strain diagrams (not shown here), all investigated samples fractured already in the elastic regime without macroscopically showing plasticity. However, on a microscopic scale, the local situations could be very different. For illustrating local differences, Fig. 12 shows typical fracture topographies for pure Al deposits as well as for Al-SiC_{CP3} and Al-SiC_{FP3} composites. In the case of the pure Al deposit in Fig. 12a, the fracture surface shows a mixture of areas that were well bonded and heavily deformed under tensile loading (green arrow) and others that remain rather smooth, more or less simply compressed and not bonded particle-particle interfaces (red arrow). In the selected micrograph, about more than 30 % of the interface appears to be well bonded. In the case of the Al-SiC_{CP3} and Al-SiC_{FP3} samples depicted in Fig. 12b and 12c, respectively, most of the SiC particles are loosely bonded or embedded within the Al matrix, as indicated by the gaps (yellow arrow) at the Al-SiC_p interfaces. Only some of these local dissimilar interfaces appear well bonded, showing plastic features on Al sites, as shown by orange arrow. This indicates that most of the plastic deformation during tensile testing occurs within the Al matrix. A particular example is given by the blue highlighted curve and the black arrow in Fig. 12b, showing details of the larger craters left by removed coarse SiC particles, as well as fractured ones in the vicinity. As compared to Al-SiC_{CP3}, the fracture surface of the Al-SiC_{FP3} deposit

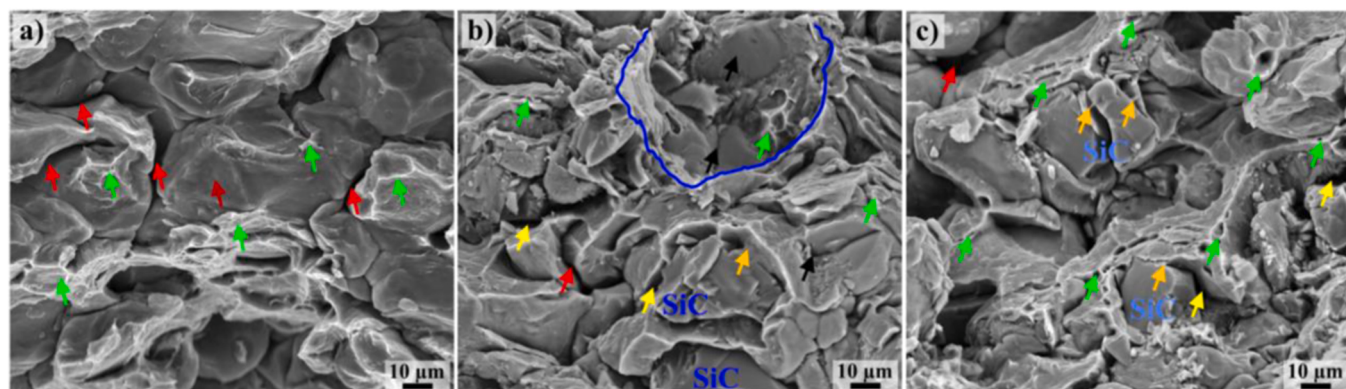


Fig. 12. Fracture surfaces of (a) as-sprayed Al, (b) Al-SiC_{CP3} and (c) Al-SiC_{FP3} deposits after tensile testing.

reveals more rupture features within the Al-matrix (green arrow). For both composites, in contrast to the pure Al-deposit, fewer non-bonded interfaces between Al-splats are observed. This may be attributed to slightly higher amounts of adiabatic shear instabilities (ASI), in agreement with the normalized UTS at higher hard phase contents.

3.5. Microstructures of graded Al-SiC composites

In contrast to the processing of homogenous composites using individually fixed SiC_P delivery rates, the graded Al-SiC_P deposits were produced by increasing the delivery rates from 0 to 3 rpm layer by layer, following the principle illustrated in Section 2.3 (see Fig. 2 b₀₋₃). Data on parameter sets are given in Table 2.

3.5.1. Graded Al-SiC deposit containing coarse hard phase

Fig. 13a shows the microstructure of the four-layer graded Al-SiC_P deposit as obtained by increased SiC_P feed rates. The SEM micrograph and EDS mapping by SEM applied to $\text{Si}_{\text{K}\alpha}$ radiation (Fig. 13b) reveal some differences in local distributions. However, the variation of SiC_P contents over the layer thickness is less defined than expected. This could probably be attributed to inhomogeneities within the individual layers, similar to those observed in uniformly processed deposits. Possible alignments of SiC_P depleted zones might superimpose the layer by layer-adjusted changes in phase compositions. According to Fig. 13a, the transition between the individual layers is smooth and barely detectable by OM, showing no defect accumulation at interlayer interfaces. Thus, it can be assumed that CS of graded composites is not impaired by defects and low interlayer cohesion. For general deposit appearance, it is worth noting, that most of the SiC_P reinforcements are intact. However, similar to the uniform composites (compare Fig. 7), some porosity is observed within the Al matrix, which to a certain extent can be attributed to fragmented SiC_P or pull-out of SiC_P during cross-section preparation.

3.5.2. Graded Al-SiC_P deposit containing fine hard phase

Fig. 14 shows cross-sectional images of the microstructure of the graded Al-SiC_{FP} deposit containing the fine hard phases. SEM and EDS results reveal the graded distribution of SiC_{FP} contents in the Al matrix and the respective increase over deposit layers. Four distinct layers can be distinguished, as depicted by red dashed lines in Fig. 14. According to area analyses by SEM/BSE-contrast and EDS mapping, the four layers from bottom to top contain SiC in amounts of 0, 3.1, 7.8 and 11.1 vol%. The corresponding layer thickness is determined to be 0.32, 0.44, 0.48, and 0.55 mm, respectively. Related results are plotted in Fig. 15 and demonstrate that conditions for deposition of uniform composites (compare Fig. 9a-9b) can be transferred to defined processing of graded

materials. It might be noted that the whole deposit has been subjected to tamping by hard reinforcements of SiC_{FP} during deposition. Such might support work hardening and in addition result in rather low porosity (compare Fig. 7, 13).

As shown in Fig. 15, within the present powder feed rate regime with low SiC_P contents, the embedded amounts show a nearly linear increase over the different spray layers and thus deposit thickness. With this, the composite's properties are expected to vary layer-by-layer. As in homogenous composites, the thickness of individual layers increases with the rising amounts of deposited carbides. Comparing the results for large and fine SiC_P, it appears that the hard phase size selection is crucial for preventing SiC_P rebound and fracture. Also, reproducible and reliable powder feeding characteristics of both materials are important to control composition gradients and to minimize depleted zones as well as to maximize SiC_P contents.

4. Discussion

The results demonstrate that uniform Al-matrix composites can in principle be manufactured by using two independent powder feed lines. The study proves that conditions for depositing uniform composites can be transferred to the manufacturing of graded materials. By that, the associated flexibility in varying individual feed rates allows producing composites with graded hard phase contents and thus graded properties. As demonstrated for electrical conductivity, hardness and strength, deposit properties can be adjusted by selected hard phase contents. For processing uniform Al-SiC_P composites, several prerequisites must be fulfilled. Attainable microstructures and properties, apart from process parameters, also depend on powder sizes as well as on powder feeding rates. The hard phase sizes become significant for avoiding rebounds or fractures and to ensure the right ratio for getting embedded into the Al-matrix. In the present study, the Al-SiC_{FP} composites manufactured by similar sizes of SiC_P and Al-powders exhibit a dense and homogenous microstructure, and better properties than those fabricated using coarser hard phase powder. The composites processed with coarse SiC_P powder suffer from hard phase fracture, rebounds and inhomogeneous feeding, the latter causing local SiC_P depletion playing a role mainly at low feed rates (see detailed micrographs in Fig. 7). Thus, only for similar sizes of SiC hard phase and Al matrix powders, conditions for uniform coating formation could be transferred to the manufacturing of graded deposits. In the following, some key points for the prerequisites are discussed in more detail.

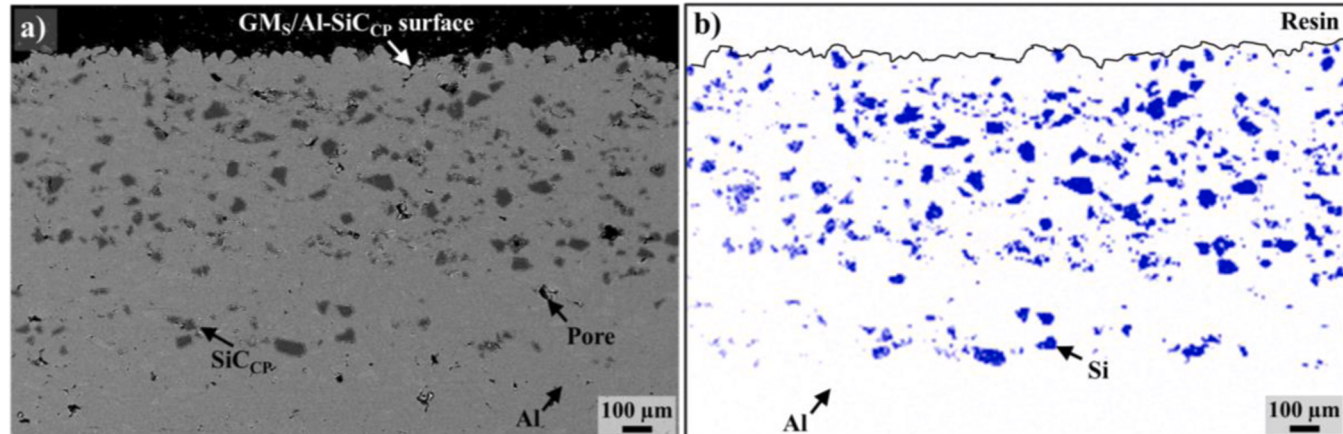


Fig. 13. Microstructures of graded composites containing coarse SiC_P, (a) OM and (b) EDS mapping of Si element. The substrate is not shown here.

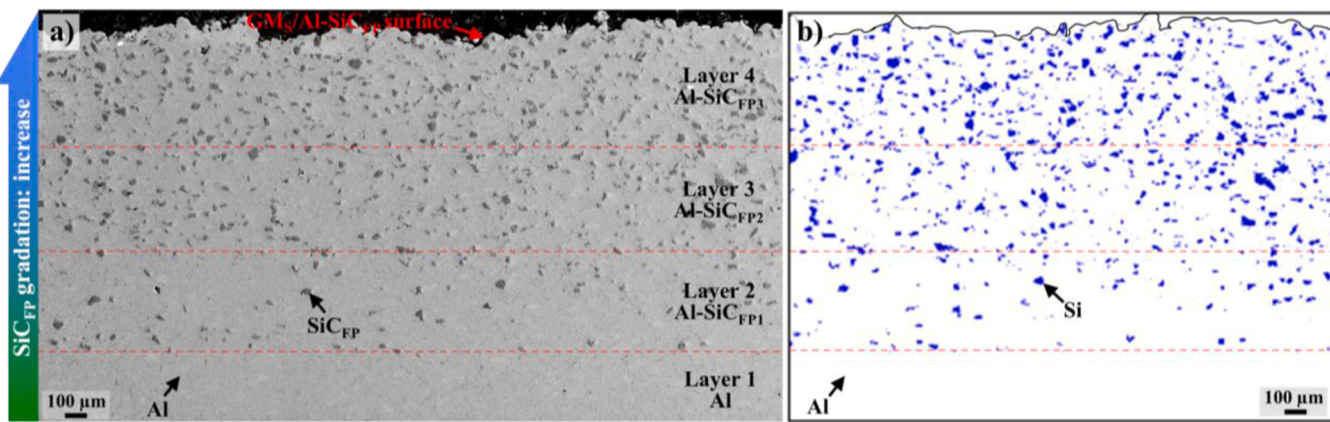


Fig. 14. Microstructures as obtained by OM (a) and EDS-mapping (b) of the (a-b) GM/Al-SiC_{FP} deposited by four graded layers with Layer 1: pure Al, Layer 2: Al-SiC_{FP1}, Layer 3: Al-SiC_{FP2}, and Layer 4: Al-SiC_{FP3}. The substrate is not shown here.

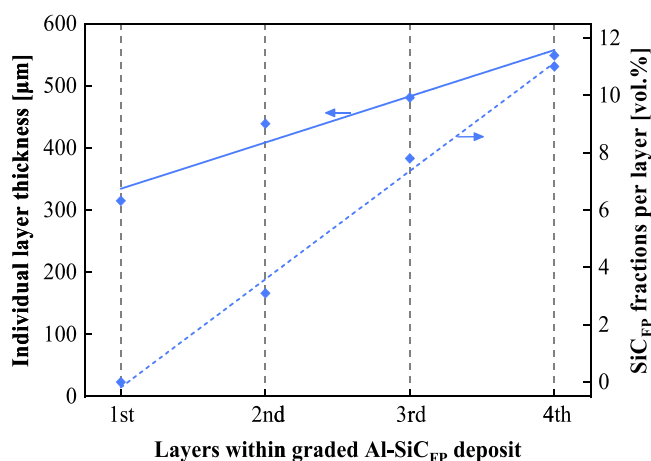


Fig. 15. Correlations of the individual layer thickness (left ordinate) and SiC_{FP} fractions (right ordinate) with the corresponding layer in the graded Al-SiC_{FP} deposit.

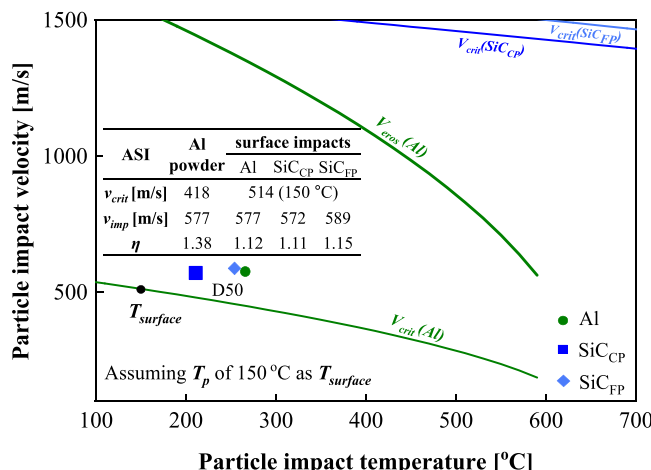


Fig. 16. Particle impact conditions and critical velocities for Al and SiC powders cold sprayed with $p_{gas} = 3$ MPa and $T_{gas} = 500$ °C as calculated by KSS software. The inserted table contains data on individual particle velocities and critical velocities as well as corresponding η -ratios at Al-particle and Al-surface sites. Critical velocities for causing ASI on the surface are calculated by assuming a surface temperature of 150 °C.

4.1. Impact conditions and ability to form areas of shear instability under dissimilar impacts

The selected cold spraying parameter sets for ensuring long-term process stability with an η -value of about 1.38 (see Section 2.2) provide good results in depositing pure Al-layers, as determined by coating cross-sections and attained low porosities (Fig. 4). However, under co-deposition of different SiC_P sizes, it becomes evident that deposit build-up needs also to consider bonding features that could be caused on the surface by hard phase impacts. To a certain extent, the bonding of hard phases could be attributed to the ability to cause areas of instability on Al-sites at the surface. Respective particle impact conditions and the critical conditions for bonding in CS can be supplied by the window of deposition based on KSS software, as given in Fig. 16 for the different mean sizes (D50).

By interpreting the ability to form ASI in terms of relative velocities and local temperatures of the ductile component, the η -values could be individually distinguished for Al powder and the Al surface under different particle impact scenarios. Whereas the η -values of Al powders are given by the impact conditions (v_p and T_p) and critical velocity at the given particle temperature (T_p), the deformation of the surface has to be considered by correlating particle velocities to critical velocities at respective surface temperatures. Despite the individual dependencies on robot kinematics and stand-off distance, the surface temperature is assumed to be $T_{surface} = 150$ °C. The corresponding results are given in the table inserted in Fig. 16, showing the different impact and critical velocities as well as η -values for Al powder and Al on deposit surface under impacts by Al, SiC_{CP}, and SiC_{FP} particles. By using larger hard phases (Al-SiC_{CP}), attained composites are more porous (Fig. 9d) and show lower electrical conductivity (Fig. 10a), as well as lower microhardness (Fig. 10b) and UTS (Fig. 11) than those co-deposited with SiC_{FP} reinforcements of similar size as the Al-particles. Part of that can be explained in terms of causing areas of instability on Al-sites on the surface. The impact velocities of the smaller hard phase SiC_{FP} powders are higher than those of the coarse SiC_{CP} ones. As a result, higher η -values are achieved that account for more shear instabilities of Al in the deposit surface. Apart from that, the coarse SiC_{CP} powder shows tendencies for fracture upon impact, as well as for leaving larger craters if rebounding. Such contributes to porosity and reduced interface bonding quality, and associated unfavorable effects on composite conductivity, microhardness and UTS. The estimation of η ratios for different impact scenarios can only provide the first guess. In reality, the effects of the missing deformation of the hard phases must also be considered. It is expected the localization of all deformation to Al as a soft component in the surface results in locally higher strain rates. This

could be beneficial for ASI formation. Vice versa, the same holds true for Al-particles hitting hard phase areas on the surface.

However, the experimental results on deposit properties for the different compositions and hard phase sizes also does not allow for a clear distinction between the various influences. Regarding conductivity, hardness and strength, advantages of composite properties could be proven mainly for hard phase contents higher than 10 vol%. At low hard phase contents, the conductivity of the Al-matrix is lower than that of the pure deposit, which is probably due to induced defects as non-bonded interfaces and higher porosities. With increased SiC-contents, the electrical conductivity of the Al-matrix improves, which indicates better bonding between the metal splats. Such could be attributed to shot peening effects by hard phase impacts. Associated lower porosity and work hardening should affect the deposit hardness. However, the measured data only show limited variation. This could indicate that the higher degree of metallic matrix deformation by higher hard phase contents reduces local recrystallization temperatures and thus affects work hardening. The reduction of deposit strength by incorporating hard phase indicates that dissimilar interfaces are less well-bonded and more prone to failure. In addition, in agreement with conductivity data, low hard phase contents seem to contribute to more defects in the metallic matrix. However, the deposit strengths then increase with higher hard phase contents. According to fracture morphologies, this is mainly due to better bonding within the Al-matrix. In addition, the strength seems also to be influenced by the improved quality of dissimilar interfaces under locally higher shear rates in depositing composites. In summary, knowledge about all these influences helps in designing the needed composite material and needed gradients for adjusting desired property ranges by cold spraying.

4.2. SiC_P contents and deposition efficiencies

Under ideal conditions, hard-phase contents should scale with the amounts fed into the system. However, non-successful hard-phase impacts can cause significant deviations from ideal conditions, ultimately running into a saturation regime [37]. This can be attributed to the effects of hard phase contents on overall and individual deposition efficiencies of metallic and hard phase components [37]. Apart from content, in the present case, the deposit thickness of uniform composites also depends on hard phase size. In the case of using Al and hard phase powders of similar sizes, the higher amount of material by increased feed rates results in a continuous rise of the layer thickness of the Al- SiC_{FP} deposits. In contrast, for the coarse SiC_P , higher SiC_{CP} feed rates result in less increase in layer thickness, which might even run into a saturation limit (Fig. 9b). As already observed for the thinnest Al- SiC_{CP} sample (Fig. 7a-b), many large SiC particles rebound during the impact.

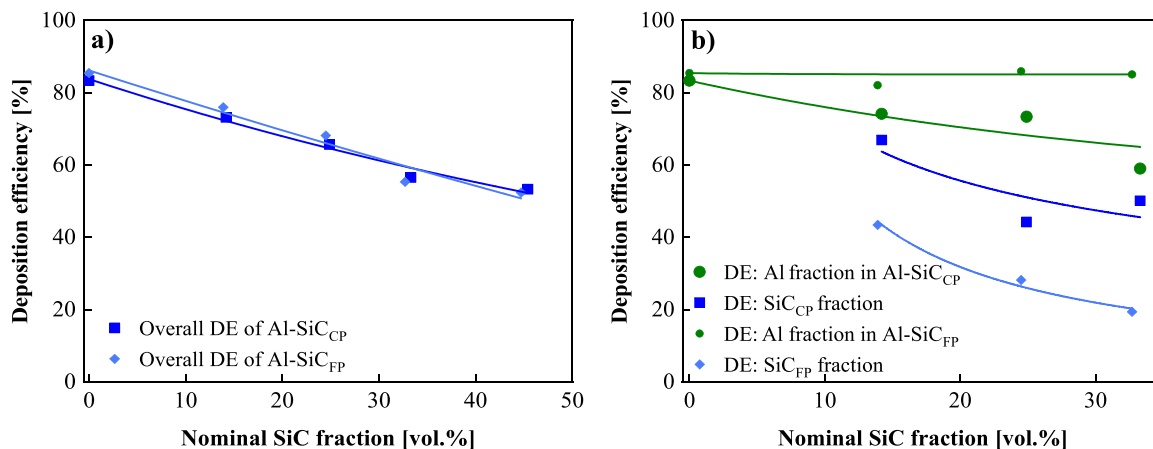


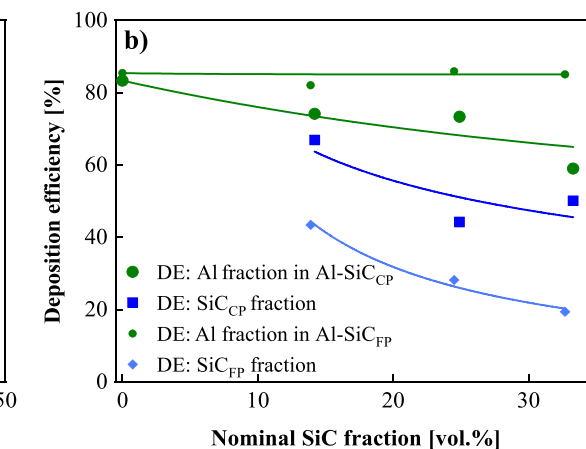
Fig. 17. Deposition efficiencies for increasing nominal hard phase contents. (a) overall deposition efficiencies and (b) individual depositions efficiencies for Al and SiC hard phase particles. Details calculations for DEs are shown in Supplementary section 6.

The loss of large hard phase particles scales with the reduction of mean sizes from 74 μm in the as-received powder to a median size of approx. 36 μm within the deposit (see Fig. 9e). The rebounds of large hard phase particles are also associated with surface damage. Observations of the top layer surface reveal locally eroded areas (see inset of Fig. 7b), in some cases leaving particle remnants or fragments at impact craters. The decrease of mean hard phase sizes during deposition is likely due to two factors. On the one hand, as given above, the large SiC_{CP} particles by their high inertia cannot reach the needed velocities to cause ASI on Al surfaces [37]. On the other hand, incoming smaller Al particles are not able to cover and thus trap large size, non well-bonded SiC_{CP} particles. Thus, it can be assumed that these large SiC_{CP} particles mainly show fracture or rebound behaviors, leaving either small fragments on the surface or causing deformation craters.

With data on present feed rates, the measured fractions of SiC_P in the deposits given in Fig. 9a can be translated to deposition efficiencies. Accordingly, Fig. 17 shows the overall and individual deposition efficiencies during the composite build-up for increased SiC contents. As plotted in Fig. 17a, the overall DEs of both powder size combinations decrease with increasing delivery rates. Similar is observed by Irissou et al. [30], by increasing the weight fraction of alumina as a reinforcing phase in the cold spraying feed powder causes a decrease in deposition efficiency. Spencer et al. [28] hypothesized that the decrease in DEs of the composite coating with an increasing weight fraction of ceramics in the feed powder is caused by rebounding of ceramic particles from the substrate. In the first instance, this can be explained by rebounding of ceramic particles just by increased hard phase to hard phase interaction. Increasing the weight fraction of SiC_P , increases the probability to hit hard phases being on the surface and thus non-bonding conditions. Thus, a greater probability for particles to deflect, rather than adhere to the Al matrix, results in a decrease in deposition efficiency [37].

More information on local situations upon particle impacts in forming the composite is provided by the individual deposition efficiencies of the associated constituents given in Fig. 17b. In using similar SiC_{FP} and Al powder sizes, the individual DE of Al remains rather constant at about 80 % with increasing SiC_{FP} contents. This indicates that almost all impacting Al particles meet surface conditions that allow for bonding, despite the local presence of soft or hard phases on the surface. In contrast, the deposition efficiency of SiC_{FP} is already rather low at small feed rates and further decreases with higher nominal hard phase contents. This can be explained by increased probabilities of impacts onto already adhering hard phases or not meeting sufficient conditions for bonding to a phase mixture at the surface.

The situation is different for co-deposition of Al and coarser SiC_{CP} powders. In this case, the individual deposition efficiencies of the SiC_{CP} are higher than those of the fine one and show a slightly slower decrease



with SiC_CP content. However, here the deposition efficiencies of Al also decrease with increasing nominal hard phase contents, as indicated by the thinner Al-SiC_{CP} sample thickness (Fig. 9b) and higher SiC_{CP} contents in the individual deposits (Fig. 9a). The lower amount of bonded Al under elevated coarse SiC_{CP} contents has several reasons. i) Non-successful coarse hard phase particle impacts can erode bonded Al from the surface. ii) Meeting empty impact craters left by non-successful SiC impacts, the following smaller Al particles (refer Fig. 3) hit surface topographies that correspond to considerable deviations from ideal, perpendicular conditions on Al, thus leading to lower bonding quality and thus increased porosity (Fig. 9d), or even rebounds. iii) Similar, non-ideal conditions will be present during the impact onto large, angular SiC_{CP} on the surface. This becomes even more difficult by ensuring dissimilar bonds to the ceramic phase. iv) Due to large hard phase extents on the surface, it is more difficult to meet sufficiently high levels of Al to ensure defined bonding conditions. All of these features result in less deposit thickness than expected at increased hard phase feed rates (Fig. 9b) and higher amounts of defects as porosities or loosely bonded particles, particularly SiC_{CP} fragments (blue arrows in Fig. 7).

It is likely that local hard phase distributions and deposition efficiencies are also affected by the homogeneity in powder supply by the conveyor disc (see Supplementary Fig. S2a). The spread of inhomogeneities could be correlated to the traverse speed of the robot and thus a pulse-like conveyance of SiC_{CP}. According to their flowability (see Supplementary, Section 3), the SiC_{CP} powders are partially conveyed in a pulse-like manner. The analyses of surface pattern formation and local inhomogeneities in microstructure could supply information for improving the effectiveness of powder feeding. Several factors influence the powder feed rate: i) disc modification for improving SiC_{CP} flowability by an alternative type and volume of feeder disc (number of holes and design of feeder discs); ii) less angular morphologies to improve flowability and apparent density of powders.

4.3. Comparison of SiC_P contents in the deposits for different process conditions

Fig. 18 summarizes data from the literature for cold spray Al-SiC composites with different hard phase contents from mechanically blended feedstock powders and the obtained volume fractions in the final deposits, together with the results from this study. The dashed line with slope one indicates the ideal case that 100 % of the nominal SiC_{CP} content is embedded into the deposit. By brittle behavior and ensuring fewer areas of shear instabilities at common interfaces, the reinforcement contents in the composites are generally lower than those of the

feedstock [18–20,22]. The content of SiC_{CP} in the deposits can reach a maximum value of about 40 vol% [20,21]. The plotted curves for individual data sets have different slopes and reveal significant differences in the co-deposition behaviors for various powder combinations, which can be attributed to different powder sizes and shapes, as well as to spray conditions. Only in one study, by using a rather low content of SiC_{CP} in the powder mixture (15 vol%), a higher fraction was observed in the deposit (21.2 vol%) [21]. In addition to powder sizes, morphologies and spray parameters, the achievable SiC_{CP} contents also depends on the types of Al matrix [38,39] and their deformation behaviors and critical particle impact conditions for bonding. It is worth noting that this crude comparison between the literature data and the present work reveals that the achievable ceramic contents in the deposits by using two powder feed lines fall within the regimes obtained by using pre-mixed powder blends for cold spraying. This justifies the present approach to using independent powder feeding for increased flexibility in adjusting the needed compositions.

4.4. Comparison of process strategies for fabricating graded Al-SiC composites

So far, the production of graded metal-ceramic composites is still challenging, with individual advantages and limits of the so far applied techniques. For supplying an overview, the typical methods of fabricating functionally graded Al-SiC_{CP} composites and respective key data are compared in Table 3. As the solid-state technique, powder metallurgy (sintering, hot isostatic pressing) was reported to enable a relatively wide regime with SiC_{CP} contents ranging from 0 to 60 vol% [9,10]. However, due to high working temperatures, the formation of undesired ternary carbides or intermetallic phases at Al-SiC interfaces could not be completely suppressed. Centrifugal casting [4–7], metal infiltration processes [8] and laser melting injection [14] operate with molten Al-alloys. This guarantees dense microstructures and defined SiC_{CP} distributions, but higher temperatures have to tackle more problems of undesired carbide and intermetallic phase formation at the interfaces. The friction stir process [40,41] operates below the melting temperature using a consumable rod of Al, in which the drilled holes are filled with ceramics. That in principle allows depositing Al-ceramic composites in individual layers of different compositions. However, by the nature of such deposition process with adjusted layer thickness and limited stir effects without a tool probe, the method has limitations with respect to adjusting defined gradients in composition, irrespective of the used SiC concentrations or sizes. The strategies for powder injection need future improvement. Spark plasma sintering can be adjusted to operate below the melting temperatures of Al-alloys and offers benefits by short sintering times [42,43]. For the example of Al-SiC composite, fully dense ultrafine microstructures of functionally graded composites were obtained [42]. However, the technique has limitations with respect to homogeneous temperature distributions, which could lead to heterogeneous microstructures of the sintered samples [43].

In comparison to so far used techniques, dual powder feeder-based cold spraying appears as an interesting, flexible alternative to process graded composites. By adjusting individually different powder delivery rates, this method can allow for the deposition of various mixtures to yield functionally graded structures over the deposit buildup. Benefits of cold spraying concern the low working temperatures, high production efficiencies and a high variety with respect to sample dimensions and geometries, which could contribute to developing strategies for additive manufacturing of graded composites. Disadvantages of cold spraying might concern limits in reaching high hard phase contents in the composite and often non-sufficient internal interface cohesion. Judging from literature data, a maximum of about 40 vol% of SiC_{CP} can be reached in homogeneous or graded composites. Slight improvements might be expected by appropriate adjustments of powder sizes and further parameter optimization of the co-deposition process (compare Section 4.2). The quality of internal interface cohesion to reach better mechanical and

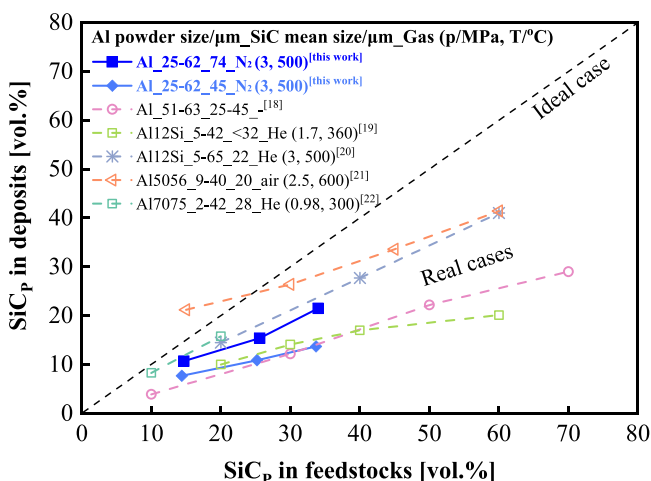


Fig. 18. Comparison of attained SiC_P volume fractions within differently cold sprayed AMCs deposits as a function of the ceramic contents in the feedstock powder.

Table 3Comparison of methods for processing graded Al-SiC_p composites.

Metal matrix	SiC vol %	Methods	Operating temperature, T/°C	Remarks	Ref.
AlSi ₁₀ Cu _{4.5} Mg ₂	1.9–36	Centrifugal casting	850	Low centrifugal speed of 1500 rpm leads to a smoother gradient than 2000 rpm, but with pronounced defects of pores	[4]
Al	0–55		725	SiC sizes affect the particle concentration, more particles were obtained in the outer zones for large particles because of their higher centrifugal force.	[6]
Al356	0–45		750–760	A wider freezing range of the matrix alloy causes a smoother transition from SiC _p enriched to depleted zones.	[7]
Al2124	0–40				
Al6061	40–60	Infiltration	above T_m	Infiltrated graded Al-SiC composites feature a dense and pore-free microstructure with a varying SiC _p distribution.	[8]
Al2124	0–44	Powder metallurgy	500	Vibration process provides a continuous SiC distribution by breaking up coarse SiC agglomerates.	[9]
Al2024	0–60		560	Four-layer sample showed a porosity of 1.4 % and the presence of Al ₄ C ₃ , CuAl ₂ , and CuMgAl ₂ .	[10]
Al6061	0–4.8	Laser melting injection	above T_m	In-situ reactant Al ₄ C ₃ platelets and acicular Al ₄ SiC ₄ were observed at SiC/Al interfaces and in Al-matrix, respectively.	[14]
Al6082	5–30	Friction surfacing process	below T_m	Multi-layering enables tailoring graded deposit composition, but SiC concentration was resulted by poor material flow.	[41]
Al	0–55	Spark plasma sinter	Up to 600	Homogeneous distribution of SiC and no deleterious phases were identified.	[43]
Al	0–11.1	Cold spraying	below T_m	A graded structure is obtained by using the fine SiC _p powder, analogous to the size of Al.	This work

thermal properties might be improved by deposit post-treatments, in the simplest case just annealing. In the present example, the deposit was stepwise graded. Smoother gradients could be obtained by finer adjustments of powder feed rates in combination with refined kinematics for reaching smaller individual layer thickness.

5. Summary and conclusions

The present study demonstrates that using two powder feed lines in cold spraying can be used as an appropriate additive-manufacturing tool for depositing Al-SiC_p composites. The individual deposit features for different hard phase contents are similar to those obtained by using premixed powder blends. However, in contrast to the use of powder blends, the given flexibility of adjusting individual feed rates allows for better fine-tuning of hard phase contents and for an easy build-up of multi-layer graded composites.

Ideal pre-requisites for homogenous composite formation are similar sizes of Al and hard phase powder, as well as appropriate spray parameter sets. In principle, the use of coarser powder as reinforcement for Al-matrix composites is possible but leads to deposit inhomogeneities as well as internal defects. Al and SiC powders in similar sizes result in a more uniform hard phase and rather well-defined hard phase distribution in the deposits, thus leading to the defined functional properties such as electrical conductivity or hardness. Differences in individual deposition efficiencies, as well as their decrease with higher hard phase contents can be explained by respective particle surface interactions and required conditions to reach bonding by adiabatic shear instabilities.

The conditions for producing homogeneous deposits were transferred to the deposition of a four-layer graded Al-SiC_p composite with dense and pore-free microstructures over the whole compositional range. Thus, cold spray co-deposition using individually tuned powder feed lines is a major step toward additive manufacturing of well-defined graded composites. Individual compositions and finer gradients can be adjusted by powder feed rates and robot kinematics. With well-tuned parameter sets, the basic principle can be also transferred to other material combinations, e.g., metal-metal (Cu-W, Cu-Mo, Ti6Al4V-Steel, etc.) or metal-ceramic (Ni-Al₂O₃, Ti-TiC, etc.). The individual performance of such graded composites, however, has to be further evaluated, and if needed, adjusted by post-treatments.

CRediT authorship contribution statement

Chunjie Huang: Methodology, Investigation, Formal analysis, Data

curation, Conceptualization, Software, Validation, Writing - original draft, Writing - review & editing. **Alexander List:** Methodology, Investigation, Writing - review & editing. **Levke Wiegler:** Investigation. **Matthias Schulze:** Investigation. **Frank Gärtner:** Supervision, Resources, Project administration, Funding acquisition, Writing - review & editing. **Thomas Klassen:** Supervision, Project administration, Writing - review & editing.

Declaration of Competing Interest

The authors declare that they have no known competing financial interests or personal relationships that could have appeared to influence the work reported in this paper.

Data Availability

Data will be made available on request.

Acknowledgments

The author Dr. Huang acknowledges the financial support of the Alexander von Humboldt Foundation. The authors also sincerely thank their dear colleagues from the HSU team for support in this work, namely (in alphabetical order) T. Breckwoldt, J. Gutierrez, M. Hartmann, M. Kollmeier, and C. Schulze for help in the sample preparation and microstructural analyses.

Appendix A. Supporting information

Supplementary data associated with this article can be found in the online version at doi:10.1016/j.addma.2022.103116.

References

- [1] R.B. Wu, K. Zhou, C.Y. Yue, J. Wei, Y. Pan, Recent progress in synthesis, properties and potential applications of SiC nanomaterials, *Prog. Mater. Sci.* 72 (2015) 1–60.
- [2] M. Occhionero, R. Hay, R. Adams, K. Fennelly, Aluminum silicon carbide (AlSiC) for cost-effective thermal management and functional microelectronic packaging design solutions, *Ceram. Process Syst. Corp. Chart. MA* 02712 (2000).
- [3] B. Saleh, J.H. Jiang, R. Fathi, T. Al-hababi, Q. Xu, L.S. Wang, D. Song, A. Ma, 30 Years of functionally graded materials: an overview of manufacturing methods, applications and future challenges, *Comp. Part. B* 201 (2020), 108376.
- [4] A.C. Vieira, P.D. Sequeira, J.R. Gomes, L.A. Rocha, Dry sliding wear of Al alloy/SiCp functionally graded composites: influence of processing conditions, *Wear* 267 (2009) 585–592.

- [5] I. Milosan, T. Bedo, C. Gabor, D. Munteanu, M.A. Pop, D. Catana, M. Cosnita, B. Varga, Characterization of aluminum alloy-silicon carbide functionally graded materials developed by centrifugal casting process, *Appl. Sci.* 11 (2021) 1625.
- [6] I.M. El-Galy, M.H. Ahmed, B.I. Bassiouny, Characterization of functionally graded Al-SiCp metal matrix composites manufactured by centrifugal casting, *Alex. Eng. J.* 56 (2017) 371–381.
- [7] T.P.D. Rajan, R.M. Pillai, B.C. Pai, Characterization of centrifugal cast functionally graded aluminum-silicon carbide metal matrix composites, *Mater. Charact.* 61 (2010) 923–928.
- [8] K.M.S. Manu, V.G. Resmi, M. Brahmakumar, P. Narayanasamy, T.P.D. Rajan, C. Pavithran, B.C. Pai, Squeeze infiltration processing of functionally graded aluminum-SiC metal ceramic composites, *Trans. Indian Inst. Met.* 65 (2012) 747–751.
- [9] C. Lin, C. Bathias, H.B. McShane, R.D. Rawlings, Production of silicon carbide Al 2124 alloy functionally graded materials by mechanical powder metallurgy technique, *Powder Metall.* 42 (1999) 29–33.
- [10] F. Erdemir, A. Canakci, T. Varol, Microstructural characterization and mechanical properties of functionally graded Al2024/SiC composites prepared by powder metallurgy techniques, *Trans. Nonferrous Met. Soc. China* 25 (2015) 3569–3577.
- [11] E. Acar, M. Aydin, Damping behavior of Al/SiC functionally graded and metal matrix composites, *J. Asian Ceram. Soc.* 9 (2021) 578–585.
- [12] M. Gui, S.B. Kang, 6061Al/Al-SiCP bi-layer composites produced by plasma-spraying process, *Mater. Lett.* 46 (2000) 296–302.
- [13] S.M.L. Nai, M. Gupta, Synthesis of Al/SiC based functionally gradient materials using technique of gradient slurry disintegration and deposition: effect of stirring speed, *Mater. Sci. Tech.* 18 (2002) 633–641.
- [14] B. Xu, P. Jiang, S.N. Geng, Y. Wang, J. Zhao, G. Mi, In-situ reactions and mechanical properties of 6061 aluminum alloy weld joint with SiCp by laser melting injection, *Mater. Des.* 203 (2021), 109538.
- [15] C.J. Huang, A. List, J.J. Shen, B.L. Fu, S. Yin, T. Chen, B. Klusemann, F. Gärtner, T. Klassen, Tailoring powder strengths for enhanced quality of cold sprayed Al6061 deposits, *Mater. Des.* 215 (2022), 110494.
- [16] C.J. Huang, M. Arseenko, L. Zhao, Y.C. Xie, A. Elsenberg, W.Y. Li, F. Gärtner, A. Simar, T. Klassen, Property prediction and crack growth behavior in cold sprayed Cu deposits, *Mater. Des.* 206 (2021), 109826.
- [17] C.J. Huang, X.C. Yan, C.Y. Chen, Y.C. Xie, M. Liu, M. Kuang, H.L. Liao, Additive manufacturing hybrid Ni/Ti-6Al-4V structural component via selective laser melting and cold spraying, *Vacuum* 151 (2018) 275–282.
- [18] G.L. Eesley, A. Elmoursi, N. Patel, Thermal properties of kinetic spray Al-SiC metal-matrix composite, *J. Mater. Res.* 18 (2003) 855–860.
- [19] E. Sansoucy, P. Marcoux, L. Ajdelsztajn, B. Jodoin, Properties of SiC-reinforced aluminum alloy coatings produced by the cold gas dynamic spraying process, *Surf. Coat. Tech.* 202 (2008) 3988–3996.
- [20] M. Yandouzi, P. Richer, B. Jodoin, SiC particulate reinforced Al-12Si alloy composite coatings produced by the pulsed gas dynamic spray process: Microstructure and properties, *Surf. Coat. Tech.* 203 (2009) 3260–3270.
- [21] M. Yu, X.K. Suo, W.Y. Li, Y.Y. Wang, H.L. Liao, Microstructure, mechanical property and wear performance of cold sprayed Al5056/SiCp composite coatings: effect of reinforcement content, *Appl. Surf. Sci.* 289 (2014) 188–196.
- [22] O. Meydanoglu, B. Jodoin, E.S. Kayali, Microstructure, mechanical properties and corrosion performance of 7075 Al matrix ceramic particle reinforced composite coatings produced by the cold gas dynamic spraying process, *Surf. Coat. Tech.* 235 (2013) 108–116.
- [23] C.J. Huang, W.Y. Li, Z.H. Zhang, M.P. Planche, H.L. Liao, G. Montavon, Effect of tool rotation speed on microstructure and microhardness of friction-stir-processed cold-sprayed SiCp/Al5056 composite coating, *J. Therm. Spray. Tech.* 25 (2016) 1357–1364.
- [24] C.J. Huang, W.Y. Li, Z.H. Zhang, M.P. Planche, H.L. Liao, G. Montavon, Modification of a cold sprayed SiCp/Al5056 composite coating by friction stir processing, *Surf. Coat. Tech.* 296 (216) (2016) 69–75.
- [25] A. Sova, V.F. Kosarev, A. Papyrin, I. Smurov, Effect of ceramic particle velocity on cold spray deposition of metal-ceramic coatings, *J. Therm. Spray. Tech.* 20 (2011) 285–291.
- [26] T. Peat, A. Galloway, A. Toumpis, P. McNutt, N. Iqbal, The erosion performance of particle reinforced metal matrix composite coatings produced by co-deposition cold gas dynamic spraying, *Appl. Surf. Sci.* 396 (2017) 1623–1634.
- [27] Q. Wang, N. Ma, M. Takahashi, X.T. Luo, C.J. Li, Development of a material model for predicting extreme deformation and grain refinement during cold spraying, *Acta Mater.* 199 (2020) 326–339.
- [28] K. Spencer, D.M. Fabijanic, M.X. Zhang, The use of Al-Al₂O₃ cold spray coatings to improve the surface properties of magnesium alloys, *Surf. Coat. Tech.* 204 (2009) 336–344.
- [29] Q. Wang, N. Birbilis, H. Huang, M.X. Zhang, Microstructure characterization and nanomechanics of cold sprayed pure Al and Al-Al₂O₃ composite coatings, *Surf. Coat. Tech.* 232 (2013) 216–223.
- [30] E. Irissou, J.G. Legoux, B. Arsenault, C. Moreau, Investigation of Al-Al₂O₃ cold spray coating formation and properties, *J. Therm. Spray Technol.* 16 (2007) 661–668.
- [31] J.M. Shockley, S. Descartes, P. Vo, E. Irissou, R.R. Chromik, The influence of Al₂O₃ particle morphology on the coating formation and dry sliding wear behavior of cold sprayed Al-Al₂O₃ composites, *Surf. Coat. Tech.* 270 (2015) 324–333.
- [32] W.Y. Li, G. Zhang, X.P. Guo, H.L. Liao, C. Codet, Characterizations of cold-sprayed TiN particle-reinforced Al alloy-based composites—from structures to tribological behaviour, *Adv. Eng. Mater.* 9 (2007) 577–583.
- [33] A. Moridi1, S.M. Hassani-Gangaraj, M. Guagliano, M. Dao, Cold spray coating: review of material systems and future perspectives, *Surf. Eng.* 36 (2014) 369–395.
- [34] X.L. Xie, S. Yin, R. Raoelson, C.Y. Chen, C. Verdy, W.Y. Li, G. Ji, Z.M. Ren, H. L. Liao, Al matrix composites fabricated by solid-state cold spray deposition: a critical review, *J. Mater. Sci. Tech.* 86 (2021) 20–55.
- [35] W.Y. Li, C.C. Cao, S. Yin, Solid-state cold spraying of Ti and its alloys: a literature review, *Prog. Mater. Sci.* 110 (2020), 100633.
- [36] S. Yin, M. Hassani, Q.G. Xie, R. Lupoi, Unravelling the deposition mechanism of brittle particles in metal matrix composites fabricated via cold spray additive manufacturing, *Scr. Mater.* 194 (2021), 113614.
- [37] T. Klassen, F. Gärtner, H. Assadi, Process Science of Cold Spray, in: C.M. Kay, J. Karthikeyan (Eds.), High pressure cold spray - Principles and applications, OH, ASM International, Materials Park, 2016, pp. 35–38.
- [38] B. Samareh, O. Stier, V. Luthen, A. Dolatabadi, Assessment of CFD modeling via flow visualization in cold spray process, *J. Therm. Spray. Tech.* 18 (2009) 934–943.
- [39] A. Moridi, S.M. Hassani-Gangaraj, M. Guagliano, M. Dao, Cold spray coating: review of material systems and future perspectives, *Surf. Eng.* 36 (2014) 369–395.
- [40] R.M. Miranda, T.G. Santos, J. Gandra, N. Lopes, R.J.C. Silva, Reinforcement strategies for producing functionally graded materials by friction stir processing in aluminium alloys, *J. Mater. Process. Tech.* 213 (2013) 1609–1615.
- [41] J. Gandra, P. Vigarinho, D. Pereira, R.M. Miranda, A. Velhinho, P. Vilaça, Wear characterization of functionally graded Al-SiC composite coatings produced by friction surfacing, *Mater. Des.* 52 (2013) 373–383.
- [42] M.J. Oza, K.G. Schell, E.C. Bucharsky, T. Laha, S. Roy, Developing a hybrid Al-SiC-graphite functionally graded composite material for optimum composition and mechanical properties, *Mater. Sci. Eng. A.* 805 (2021), 140625.
- [43] N. Sharma, S. Alam, B. Ray, Fundamentals of spark plasma sintering (SPS): an ideal processing technique for fabrication of metal matrix nanocomposites, in: *Spark Plasma Sinter. Mater.*, Springer, 2019.